Fusion Science and Technology

ISSN: 1536-1055 (Print) 1943-7641 (Online) Journal homepage: http://www.tandfonline.com/loi/ufst20

The National Ignition Facility Diagnostic Set at the Completion of the National Ignition Campaign, September 2012

J. D. Kilkenny, P. M. Bell, D. K. Bradley, D. L. Bleuel, J. A. Caggiano, E. L. Dewald, W. W. Hsing, D. H. Kalantar, R. L. Kauffman, D. J. Larson, J. D. Moody, D. H. Schneider, M. B. Schneider, D. A. Shaughnessy, R. T. Shelton, W. Stoeffl, K. Widmann, C. B. Yeamans, S. H. Batha, G. P. Grim, H. W. Herrmann, F. E. Merrill, R. J. Leeper, J. A. Oertel, T. C. Sangster, D. H. Edgell, M. Hohenberger, V. Yu. Glebov, S. P. Regan, J. A. Frenje, M. Gatu-Johnson, R. D. Petrasso, H. G. Rinderknecht, A. B. Zylstra, G. W. Cooper & C. Ruizf

To cite this article: J. D. Kilkenny, P. M. Bell, D. K. Bradley, D. L. Bleuel, J. A. Caggiano, E. L. Dewald, W. W. Hsing, D. H. Kalantar, R. L. Kauffman, D. J. Larson, J. D. Moody, D. H. Schneider, M. B. Schneider, D. A. Shaughnessy, R. T. Shelton, W. Stoeffl, K. Widmann, C. B. Yeamans, S. H. Batha, G. P. Grim, H. W. Herrmann, F. E. Merrill, R. J. Leeper, J. A. Oertel, T. C. Sangster, D. H. Edgell, M. Hohenberger, V. Yu. Glebov, S. P. Regan, J. A. Frenje, M. Gatu-Johnson, R. D. Petrasso, H. G. Rinderknecht, A. B. Zylstra, G. W. Cooper & C. Ruizf (2016) The National Ignition Facility Diagnostic Set at the Completion of the National Ignition Campaign, September 2012, Fusion Science and Technology, 69:1, 420-451, DOI: 10.13182/FST15-173

To link to this article: http://dx.doi.org/10.13182/FST15-173

ANS

FUSION SCIENCE AND TECHNOLOGY · VOLUME 69 · 420–451 · JANUARY/FEBRUARY 2016

The National Ignition Facility Diagnostic Set at the Completion of the National Ignition Campaign, September 2012

J. D. Kilkenny,[a]* P. M. Bell,[b] D. K. Bradley,[b] D. L. Bleuel,[b] J. A. Caggiano,[b] E. L. Dewald,[b] W. W. Hsing,[b] D. H. Kalantar,[b] R. L. Kauffman,[b] D. J. Larson,[b] J. D. Moody,[b] D. H. Schneider,[b] M. B. Schneider,[b] D. A. Shaughnessy,[b] R. T. Shelton,[b] W. Stoeffl,[b] K. Widmann,[b] C. B. Yeamans,[b] S. H. Batha,[c] G. P. Grim,[c] H. W. Herrmann,[c] F. E. Merrill,[c] R. J. Leeper,[c] J. A. Oertel,[c] T. C. Sangster,[d] D. H. Edgell,[d] M. Hohenberger,[d] V. Yu. Glebov,[d] S. P. Regan,[d] J. A. Frenje,[e] M. Gatu-Johnson,[e] R. D. Petrasso,[e] H. G. Rinderknecht,[e] A. B. Zylstra,[e] G. W. Cooper,[f] and C. Ruiz[f]

[a]*General Atomics, La Jolla, California 92121*
[b]*Lawrence Livermore National Laboratory, Livermore, California 94550*
[c]*Los Alamos National Laboratory, Los Alamos, New Mexico 87545*
[d]*Laboratory for Laser Energetics, Rochester, New York 14623*
[e]*Massachusetts Institute of Technology, Cambridge, Massachusetts 02139*
[f]*Sandia National Laboratories, Albuquerque, New Mexico 87123*

Received July 13, 2015
Accepted for Publication August 18, 2015
http://dx.doi.org/10.13182/FST15-173

Abstract — *At the completion of the National Ignition Campaign (NIC), the National Ignition Facility (NIF) had about 36 different types of diagnostics. These were based on several decades of development on Nova and OMEGA and involved the whole U.S. inertial confinement fusion community. In 1994, the Joint Central Diagnostic Team documented a plan for a limited set of NIF diagnostics in the NIF Conceptual Design Report. Two decades later, these diagnostics, and many others, were installed workhorse tools for all users of NIF. We give a short description of each of the 36 different types of NIC diagnostics grouped by the function of the diagnostics, namely, target drive, target response and target assembly, stagnation, and burn. A comparison of NIF diagnostics with the Nova diagnostics shows that the NIF diagnostic capability is broadly equivalent to that of Nova in 1999. Although NIF diagnostics have a much greater degree of automation and rigor than Nova's, new diagnostics are limited such as the higher-speed X-ray imager. Recommendations for future diagnostics on the NIF are discussed.*

Keywords — *Target drive diagnostics, target response diagnostics, target assembly diagnostics.*

Note — *Some figures may be in color only in the electronic version.*

I. INTRODUCTION: THE LONG HISTORY OF THE NIF DIAGNOSTICS

Community experience in the measurement of high-energy-density plasmas has been accumulated over several decades on large laser and pulsed power facilities as well as at the Nevada Test Site. The scientific progress has been discussed at the biennial series of High Temperature Plasma Diagnostic (HTPD) Conferences, which started in the 1970s. The most recent HTPD conference—20th Topical Conference on High-Temperature Plasma Diagnostics (HTPD 2014)—was held in Atlanta, June 1–5, 2014. Papers presented at the conferences are comprehensively documented in special volumes of *Review of Scientific Instruments*.

Large high-energy-density experimental facilities such as the National Ignition Facility (NIF), OMEGA, and

*E-mail: kilkenny1@llnl.gov

Z have evolved since the early 1970s. In parallel with the machines, the diagnostic technologies have also evolved, as has the ability to routinely operate these diagnostics. Facility users are often not aware of the details of the diagnostics, and as a result, it is important that they be operated reliably and accurately with routine data analysis and archiving. At Lawrence Livermore National Laboratory (LLNL), experience operating a suite of diagnostics on a large laser system for users was accumulated on the Nova laser target chamber[1] that operated from 1984 to 1999, eventually having about 100 diagnostic systems. In parallel with Nova, OMEGA at Laboratory for Laser Energetics (LLE) in various incarnations and pulsed power machines at Sandia National Laboratories (SNL) have also matured as user facilities with the need for routine reliable and accurate diagnostic suites. The importance of operational and engineering support in diagnostic setup, control, data recording, analysis, and archiving for users has also evolved on the NIF. Most of the diagnostics were not in the project phase of the NIF project, but now, operating the diagnostics is a major part of the whole NIF facility operation.

Planning for NIF diagnostics began with the Nova Technical Contract (NTC) in the early 1990s, which demonstrated at Nova-scale the important parameters (such as plasma scale length and implosion convergence) needed for ignition. The scope of the National Ignition Campaign (NIC) diagnostic set evolved as the diagnostics needed for the NTC, which was at ~1/3 linear scale of NIF, were refined.[1] At that time, the Joint Central Diagnostic Team (JCDT) was formed with members from all of the U.S. Inertial Confinement Fusion (ICF) sites to coordinate efforts. Working with their home laboratories, the JCDT members developed plans for NIF diagnostics through ICF program funding at the various ICF laboratories. Commitment from the sites was largely based on the zeal of individual scientific experts in particular diagnostic disciplines at the different sites. The resulting strategy called for a national effort to develop and implement a comprehensive suite of diagnostics on NIF in a phased manner. Some need for multiple complementary diagnostics was recognized as an essential requirement because no single diagnostic makes a perfect measurement, and so there was some planned duplication where multiple diagnostics would be available to measure key observables of the experiments.

The Nova experience, together with experience from the OMEGA laser, and the pre-Z facilities at SNL provided the scientific and engineering basis for the JCDT to plan the initial set of diagnostics on the NIF. The mission of the NIF ignition program drove the measurement requirements and thus the plans for the initial diagnostic set. The first documentation of the proposed NIF diagnostics was in the NIF Conceptual Design Report[2] (CDR), which defined the scope and the initial costing of the NIF project. In the CDR, one part of the initial NIF project included target diagnostics. The initial set of target diagnostics in the CDR was defined as those required to make measurements to verify laser performance, to perform the initial ICF target experiments of measuring the drive and symmetry of the hohlraums, and to measure thermonuclear yield. The phase I diagnostics in the CDR are shown in Table I, which demonstrates the early commitment from Los Alamos National Laboratory (LANL) and SNL to support the NIF at LLNL. As NIF evolved over the two decades from the CDR to NIC completion, the national involvement broadened to also include LLE, General Atomics (GA), Massachusetts Institute of Technology (MIT), and National Securities Technology (NSTec). The Atomic Weapons Establishment (AWE) and Commissariat à l'Energie Atomique (CEA) were also involved. Apart from diagnostics to measure the laser performance, these phase I diagnostics were removed from the formal NIF project scope after a few years.

There was a period of almost 20 years between the CDR and the completion of NIC, but most of the CDR diagnostics were implemented (as described below) where the nine NIF CDR diagnostic types from 1993 and Ref. 3 are compared with actuality (italicized) in 2013.

CDR Streaked Slit Camera (SSC): Two X-ray streaked slit cameras (SSCs) were to be fielded in close proximity to a target using the first pair of ten-inch manipulators (TIMs). These cameras were to provide time-resolved X-ray images and/or spectra with a spatial resolution of ~50 μm, similar to the ones on Nova. A pair of the cameras was planned for beam synchronization activities. *On NIF, the original X-ray streak cameras were replaced by diagnostic insertion manipulator (DIM) insertable (X-ray) streak cameras (DISCs) (Sec. III.B).*

CDR Static X-Ray Imager (SXI): The static X-ray imagers (SXIs) were to be X-ray microscopes providing time-integrated images at 2.5-keV photon energy with 20-μm spatial resolution. They were to have a l-cm field of view from close to the poles of the target chamber so that X-ray images of the hohlraum laser entrance holes (LEHs) could be recorded. Together with the gated X-ray imagers, these diagnostics would be required for the beam smoothing implementation, beam pointing, and spot-size measurements. *On NIF, these became the two SXI instruments (Sec. III.A).*

CDR Time-Resolved X-Ray Imagers (GXIs): Time-resolved X-ray imagers (GXIs) were to provide time-gated X-ray images at photon energies between 2 and 10 keV with a temporal resolution of 80 ps and a spatial resolution of 5 to 10 μm. These were to be used primarily for

TABLE I

The NIF Diagnostics in the NIF CDR in 1994

Diagnostic	Acronym	Lab	Specs	Nova equivalent
Laser validation-pointing, focusing, & synchronization				
Static x-ray imager (ruggedized)	SXI	LLNL	20 μm, Wolther, axis view	KB
Streak x-ray camera	SSC	LLNL	5 ps, 50 μm, 2–5 cm field	SSC
Twelve-inch manipulator	TIM	LLNL	Universal vacuum load-lock manipulator system	SIM
Hohlraum temperature tuning and shock timing				
Soft x-ray power diagnostic	SXSS	SNL/LLNL	time-resolvedbroadband x-ray spectrometer	SOP
Shock break out systems	SOP	LLNL/SNL	time-resolved *f*/10, uv microscope active & passive	SOP
Filter flourescer	FFLEX	LLNL	high-energy x ray and spectrum 5–300 keV	FFLEX
Hohlraum, symmetry tuning				
Gated x-ray imaging system	GXI	LANL/SNL	80 ps, 5–10 μm 2–10 keV x-ray imager	GXI
Target yield	YN	SNI	10^{7}–$5x10^{20}$ activation (In,Cu)	Yield
Neutron time of flight	NTOF	LANL	10^{8}–10^{15} current mode	GCNTOP
Neutron imaging	NI	LLNL	10 μm 10^{12} DT, 10 cm TIM, M=	NPAM
Soft x-ray imager	SXRI	SNL	30 μm, 300 ps, normal multi-layer at 250 eV normal incident	GSXRFC

hohlraum symmetry tuning. Because they would be based on X-ray pinhole technology, they were to be fielded in the TIMs. *On NIF, these became the time-gated X-ray detector (GXD) and hardened (gated) X-ray imager (hGXI) (Sec. III.B), and they were fielded in the DIMs.*

CDR Soft X-Ray Power Diagnostics: The time history of the hohlraum radiation temperature was to be measured by two techniques that were successfully used on Nova. The X-ray flux escaping from a small hole in the hohlraum wall was to be measured by an absolutely calibrated, broadband, time-resolving X-ray spectrometer. This instrument was either to be similar to the Nova Dante system or to use a new technique that was tested on Saturn at SNL. The other technique was to be a soft X-ray streak spectrometer (SXSS) using a transmission grating that was not eventually implemented. *On NIF, the first of these techniques became the two Dante detectors (Sec. III.A).*

CDR Soft X-Ray Imager (SXRI): The soft X-ray imager (SXRI) was to record low-energy, gated X-ray images used to measure beam pointing, spot size, and hohlraum symmetry. *On NIF, this became a soft X-ray snout that can be added to the front of a NIF GXD.*

CDR High-Energy X-Ray (HEX) Spectrometer [Filter Fluorescer (FFLEX)]: The high-energy X-ray (HEX) spectrometer, similar to the filter fluorescer (FFLEX) diagnostic on Nova, was to be an absolutely calibrated FFLEX array used to measure the photon spectrum in various energy channels from 5 to 100 keV. *On NIF, these became the FFLEX (Sec. III.A).*

CDR Shock Break-Out Diagnostic [Streaked Optical Pyrometer (SOP)]: The shock break-out diagnostic was to be similar to the streaked optical pyrometer (SOP) on Nova. It was to provide a time-resolved measurement of the optical signal created by the shock break-out from the target. In addition to the passive system used on Nova, an active version of this system was to be designed to enable measurements over a wider dynamic range in radiation temperature. This system measures the time-resolved loss in reflectivity of a probe laser beam on a witness plate, thereby determining hohlraum radiation temperature history. *On NIF, this became the SOP. The active detector became the Velocity Interferometer System for Any Reflector (VISAR) (Sec. III.B).*

CDR Total Neutron Yield (YN) Detector: The total neutron yield (YN) was to be determined by measuring the neutron activation of various detector materials. *On NIF, these became the neutron activation detectors (NADs) (Sec. III.C.1).*

CDR Neutron Time-of-Flight (NTOF) Detector: A scintillator-based neutron time-of-flight (NTOF) detector combined into one system the functions of Nova's large area neutron scintillator array (LANSA) and the Nova ion temperature diagnostic. It was to require a collimator near the target chamber. The 10-m-diameter sized room that is required around the spectrometer was included in the building layout in what became known as the neutron alcove. *On NIF, these became the SPEC E and SPEC A NTOF detectors (Sec. III.C.2).*

CDR Neutron Imager (NI): A scintillator-based neutron imager (NI) uses apertures in a neutron-thick substrate to construct time-integrated neutron images. *On NIF this became the neutron imaging system (NIS) (Sec. III.C.1).*

The rest of this paper is structured as follows. In Sec. II the NIC proposed diagnostic Execution Plan (EP) is described and compared with the final state of the NIC diagnostics. Section III, the bulk of this paper, is a functional description of each of the 36 different types of NIC diagnostics. The descriptions are grouped by the function of diagnostics, namely, of drive in Sec. III.A; target response in Sec. III.B; and target assembly, stagnation, and burn in Sec. III.C. The locations of the diagnostics on the target chamber are discussed in Sec. IV. The important but often overlooked target diagnostic control system (DCS) is described in Sec. V.A. Comparison of NIF diagnostics with the Nova diagnostics is presented in Sec. VI. Section VII comprises a summary and conclusion. A glossary of acronyms is given in the Appendix.

II. SUMMARY OF DIAGNOSTICS UNDER NIC

II.A. Scientific Responsibility for NIF Diagnostics

There were nearly two decades of diagnostic innovation on Nova, OMEGA, and Z between the 1994 CDR and the end of NIC. In this period, there were many additions to the list of initial NIF diagnostics, some of which are summarized in review papers.[3–6]

At the completion of the NIF project, an ignition project was formed called the National Ignition Campaign. The NIC Execution Plan (EP) was first submitted to the National Nuclear Security Administration (NNSA) in 2006. It defined a set of diagnostics as part of the baseline configuration for NIF. The completion criteria were based on the concept of providing the diagnostics required to support the experimental campaigns used to verify laser performance and measure target performance as an integral part of the experimental campaigns required for ignition on the NIF. The scope of the set of diagnostics was to provide a core set of radiographic, optical, X-ray, and fusion measurement capability sufficient to support ignition, the High Energy Density Science program needs, and other user applications during routine facility operations.

Starting around 2007, a robust NIF diagnostic activity started. The JCDT had stopped functioning around 2000, but the need for diagnostic development to keep pace with the completion of the NIF project and the goals of the NIC EP drove an active series of NIF user workshops encouraging full national support of the NIF diagnostics. These NIC diagnostic workshops with attendances of about 100 began in early 2009 and were held about twice a year. The outreach process was very successful adding scientific responsibility for MIT and GA. By the end of the NIC in 2012, there were 36 different types of diagnostics (about 65 different diagnostics in total) under full facility control.

II.B. Engineering and Operations of the NIF Diagnostics

Because the NIF is a major user facility, any new diagnostics must be interfaced to the facility and must be controlled and operated by the facility computer systems. The NIF facility provides the systems in the target area necessary for executing experiments. This includes integration, qualification, control, and operation of diagnostics, as well as the target area systems necessary for executing experiments, and the requisite off-line and online testing and calibration. In addition, the first analysis of diagnostic data and archiving is done automatically by some of the facility's computer systems a few minutes after a shot.

Although all diagnostics are integrated and operated by the NIF operations and engineering staff, the responsibility for setting the specifications, design, construction, initial testing, accuracy of the diagnostics systems, and data analysis was and is shared among the NIC partners. The extraordinary contributions to NIF diagnostics by NIC partners and collaborators are described in the detailed descriptions of the diagnostics below and in the references at the end of this paper.

The magnetic recoil spectrometer (MRS) of Sec. III.C is a good example of shared responsibility. MIT developed the concept of the MRS and while working with LLE installed and tested the first MRS on OMEGA. A group of scientists and engineers led by MIT scientists set the specifications for a NIF version of the MRS. The ICF program at LLE assumed responsibility for design and fabrication of the NIF MRS at LLE. MIT, LLE, and

LLNL prepared the interfacing and alignment processes on NIF and set up the data-processing capability at LLNL. The instrument (see Fig. 1) was delivered to NIF in 2009 and commissioned in 2010. LLNL has formal environment, safety, and health responsibility; it operates the instrument, collects the data, and etches the set of plastic (CR-39) foils that contain the data. However, to this day, MIT remains responsible for the operations processes, the data analysis, and entering the processed data into the NIF data archives, and their staff are involved in the day-to-day physics studies arising from the MRS.

For all diagnostics, LLNL was and remains responsible for the major effort of installation, commission, and operation. Operation of the complete set of diagnostics requires specification of 13 000 parameters and 1000 control points and configuration control of thousands of diagnostic parameters. For NIF, the high cost of each shot dictated that the reliability of the diagnostics be extremely high relative to previous ICF systems. In order to assure that the reliability requirements were achieved, a rigorous process was used to assure that new diagnostics installed on NIF would operate properly. After off-line acceptance testing, each instrument passed a series of qualification hurdles prior to delivering certified data. The Installation Qualification (IQ) assured that the diagnostic was installed properly and that all utilities and controls were connected and functioning. The Operational Qualification (OQ), completed prior to use on target experiments, tested the full operation of the instrument against a predetermined set of requirements. The final step, Performance Qualification (PQ), verified that the diagnostic met its physics requirements. In some cases, the PQ process takes months or even years since some requirements can only be verified when the requisite conditions exist in the experiment, e.g., yield or signal/noise. This rigorous engineering has contributed to an extremely reliable suite of diagnostics on the NIF, delivering high-quality data >99% of the time.

There are about 60 major data analysis algorithms. These algorithms draw data from calibration files unique to the instrument and filters for each experiment. Many run automatically, providing processed data within minutes of a shot. Most data are archived, available, and searchable by qualified users. The NIF diagnostic control and data acquisition system is discussed in Sec. V.

II.C. The Diagnostic Manipulators on the NIF

The diversity of experimental requirements and limited diagnostic lines of sight have necessitated many of the instruments at major ICF facilities to be removable, which allows them to be installed in different port locations to support the varied user experimental configurations. This is accomplished with vacuum-interlocked DIMs that are used to place and align instruments close to the target. Starting in the 1990s (Ref. 3), a common manipulator policy was developed within the ICF program starting with the TIMs.

The DIM is an inserter and manipulator of diagnostics into the target chamber. A vacuum interlock is provided to

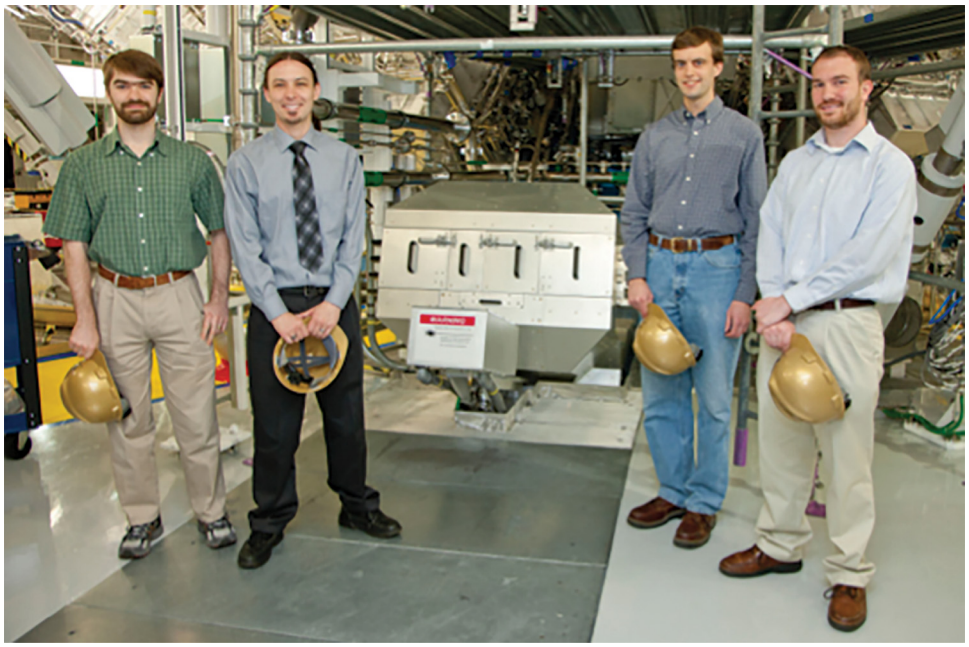

Fig. 1. The MRS is shown with four students from MIT who were key to implementing the instrument and the CR-39 detectors.

make it possible to withdraw a diagnostic from the chamber and work on it without disrupting the chamber vacuum. The concept is based on the very successful six-inch manipulators (SIMs) used on Nova and the TIMs used on OMEGA (which has six of them). The standardized interface on TIMs and DIMs has allowed movable DIM-based diagnostics to be easily tested at or borrowed from OMEGA. The French laser, Laser MegaJoule (LMJ), in Bordeaux uses the same concept with its system for insertable diagnostics (SIDs). The Trident laser at LANL uses a version of the TIM.

In the CDR, the NIF diagnostic manipulators were envisaged as being TIMs, but during the design process the bore was increased from the nominal 10 in. to ~30 cm. The DIMs are mounted to 46-cm ports on NIF with a gimbal and supported at the outboard end by a "bi-pod" positioner consisting of two motorized stages. Transverse alignment of the diagnostic in the DIM is achieved by these external bi-pods, which cause the diagnostic at the other end to pivot about the gimbal mount. The DIM is connected to the target area roughing system to pump the loading part of the DIM external to the target chamber. After the DIM is roughed down, the vacuum gate valve at the chamber port can be opened. High-vacuum pumping is done through the target chamber. The load-lock of a DIM is shown in Fig. 2.

For the duration of the NIC, NIF had three DIMs, two in the equatorial plane at (90,78) and (90,315), and one polar DIM at (0,0), where the numbers in parentheses are the theta and phi spherical coordinates in degrees. The DIM that is presently installed at (90,78) was initially at (90,45) and was moved to the chamber location (90,78) to provide improved visibility of target features. Because of user demand there are plans to install two more DIMs starting in the fall of 2016.

II.D. Engineering the Diagnostics for a Neutron Environment

The most neutron-sensitive part of some of the NIF diagnostic is a charge-coupled-device (CCD) detector such as the CCD in the GXDs and the CCD used in the SXIs. For the modest yields achieved during the NIC, the CCD is replaced by film for the SXIs, and the GXDs are replaced by hGXI, which have film as the recording medium. Some diagnostics were designed initially for operation in a much higher neutron yield environment that would result from neutron yields of $>10^{17}$. Streaked Polar Instrumentation for Diagnosing Energetic Radiation (SPIDER) and Active Readout In A Neutron Environment (ARIANE) (see below) have extensive neutron shielding and will operate at this kind of yield.

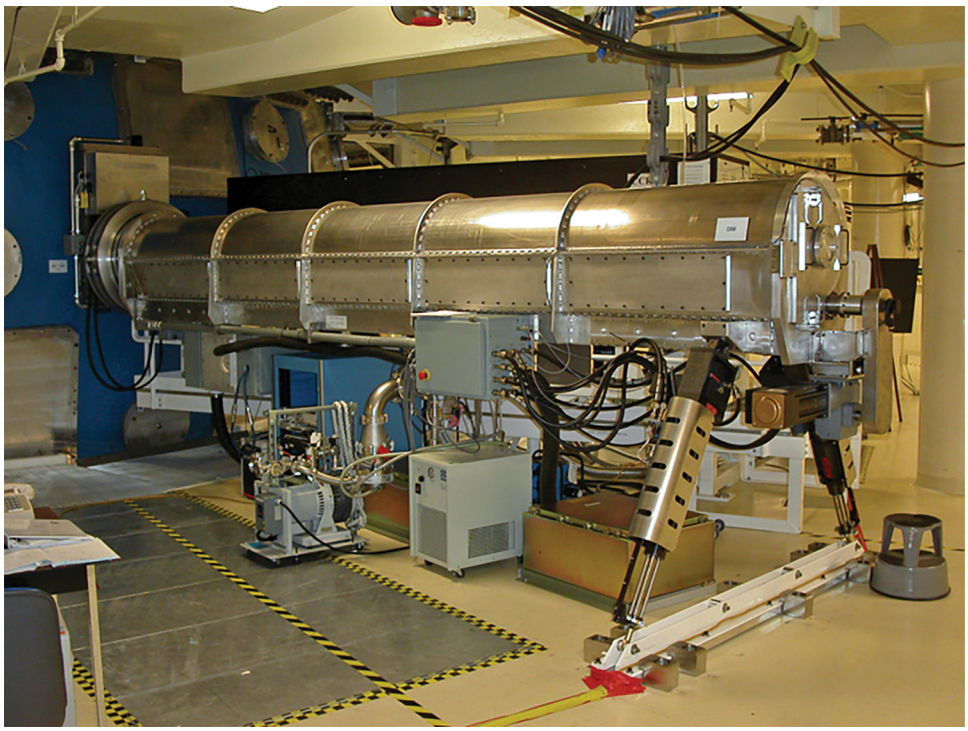

Fig. 2. The load-lock part of a DIM on the NIF. The outside of the target chamber is the blue surface on the left. The diagonal struts at the end of the tube are the bi-pods, which pivot the DIM about the gimbal located just outside the chamber wall.

TABLE II

Diagnostics of Laser Absorption and Hohlraum Conditions

Acronym	Diagnostic	Scientific Responsibility	Observable	Reference(s)
FABS31 FABS36	Full aperture backscatter station	LLNL	Backscattered light into lenses at 31 and 36 deg	7
NBI23.5 NBI31 NBI36	Near backscatter imager	LLNL	Backscattered light near lenses at 23.5, 31, and 36 deg	7
Dante1 Dante2	Broadband, time-resolved X-ray spectrometer	LLNL	Hohlraum X-ray drive conditions	8, 9, and 10
FFLEX FFLEX TR	Filter fluorescer (time resolved)	LLNL/AWE	Hot electron fraction and temperature	11 and 12
SXI-L SXI-U	Static X-ray imager	LLNL	Laser entrance hole size and beam pointing	13 and 14
EHXI	Equatorial hard X-ray imager	LLNL	Beam pointing in the hohlraum	
EMP	Electromagnetic power	LLNL	Microwave generation	

II.E. Use of Snouts on the NIF

The time-gated and time-streaked X-ray detectors that are inserted into the DIMs are used for a variety of measurements. The X-ray–sensitive parts of the detectors have instruments in front of them that either spatially resolve or spectrally disperse the X-rays onto the detectors. Because these instruments have lengths of ~50 to 100 cm and are attached to the detectors, they are called snouts. For example, the GXD discussed below is a gated detector with various pinhole snouts attached to the front of the detector where the magnification of the snout used depends on the experimental use.

III. CATEGORIZATION AND FUNCTION OF NIC DIAGNOSTICS

At the end of the NIC, the NIF was equipped with approximately 60 optical, X-ray, and nuclear diagnostics that together provide up to 300 channels of experimental data with approximately half of the diagnostics fielded on most shots.

It is customary to categorize and discuss the diagnostics on laser or pulsed power systems by their discipline as optical, X-ray, or nuclear as is done in Refs. 3, 4, and 5. A more insightful categorization is by their principal use during the three major phases of an implosion or a planar experiment. First, laser (or pulse power) energy is absorbed, thereby creating a drive (usually by shock waves), that is then applied to implode a spherical or cylindrical target or to accelerate a planar target. The target then responds to the drive, and there is target motion or shock break-out. Finally, for an implosion, the fuel assembles close to the center of the target. The convergence causes heating, and with deuterium, tritium, or ^{3}He fuel, there can be thermonuclear burn. In this major section of the paper, we categorize and discuss the NIF diagnostics in these three groupings, namely,

1. *Sec. III.A:* diagnostics of laser absorption and hohlraum conditions, also referred to as drive diagnostics
2. *Sec. III.B:* diagnostics of the shock and implosion phase, also referred to as target response/implosion diagnostics (not all experiments are implosions)
3. *Sec. III.C:* diagnostics of fuel assembly, stagnation, and thermonuclear burn.

III.A. Drive Diagnostics (Laser Absorption and Hohlraum Conditions)

The NIF diagnostics that measure the laser absorption and hohlraum conditions (specifically, the radiation drive) are shown in Table II. In Table II as well as in Tables III through VI, the scientific responsibility for the observable and the diagnostic measures are shown as well as the acronym and the reference(s).

TABLE III

Target Response/Implosion Diagnostics*

Acronym	Diagnostic	Scientific Responsibility	Observable	Reference(s)
SOP	Streaked optical pyrometer	LLNL	Shock break-out	15 and 16
VISAR	Velocity Interferometer System for Any Reflector	LLNL/LLE	Shock velocity versus time	15 and 16
DISC (3)	DIM insertable (X-ray) streak camera	LLNL/LLE	Implosion velocity and ablator thickness	17 through 20
GXD (2)	Time-gated X-ray detector	LLNL/LANL	Drive symmetry for low-yield shots	21, 22, and 23
hGXI (2)	Hardened (gated) X-ray imager	LLNL/LLE	Drive symmetry for yield $<10^{16}$ neutrons	24 and 25
NTOF4BT	Neutron time-of-flight bang time at 4 m	LLE/LLNL	Neutron BT	26
PTOF	Proton (particle) time-of-flight detector	MIT/LLNL/LLE	D-^{3}He-proton, D-D neutron, and D-T neutron BT	27 and 28
SPBT	South pole bang time	LLE/LLNL	Time of X-ray emission from the imploded capsule	29
SPIDER	Streaked Polar Instrumentation for Diagnosing Energetic Radiation	SNL/LLNL	X-ray burn history of the implosion	30
GRH	Time and spectrally resolved gamma reaction history	LANL/LLNL	Gamma spectrum and time history	31 through 34

*Numbers in parentheses indicate the number of units.

TABLE IV

Diagnostics of the Hot Spot*

Acronym	Diagnostic	Scientific Responsibility	Observable	Reference(s)
NAD-Cu	Neutron activation detector using Cu	SNL	Unscattered neutron yield from a D-T–filled capsule	35
NAD-Zr in well	Neutron activation detector (well mounted)	LLNL	Unscattered neutron yield from a D-T–filled capsule	36
NAD-snout indium (In)	Neutron activation detector (DIM mounted)	LLNL	Unscattered neutron yield from a D-D–filled capsule	37
ARIANE	Active Readout In A Neutron Environment (gated X-ray imager)	LLNL	X-ray hot spot size and shape for yields $<10^{17}$ neutrons	38
DIXI	Dilation imager for X-rays at ignition	GA/LLNL	X-ray hot spot size and shape with an X-ray gate time $\sim$10 ps	39
NIS	Neutron imaging system	LANL/LLNL	Hot spot size and fuel asymmetry	40 through 43
NITOF	Neutron imaging time of flight	LANL	Ion temperature	
NTOF20 IgnHi	Neutron time of flight	LLE/LLNL	Ion temperature	44
NTOF4 (3)	Neutron time of flight 4 m	LLE/LLNL	Ion temperature, yield	26

*Numbers in parentheses indicate the number of units.

TABLE V

Diagnostics of the Areal Density*

Acronym	Diagnostic	Scientific Responsibility	Observable	Reference(s)
CR	Compton radiography	LLNL	Fuel shape	45
MRS	Magnetic recoil spectrometer	MIT/LLE/LLNL	Neutron spectrum	46 through 49
Flange-NAD (17)	Neutron activation detector (flange mounted)	LLNL	Anisotropy of *n* scattering	37
NTOF20 SPEC A NTOF20 SPEC E	Neutron time-of-flight spectrometer	LLNL/LLE	Neutron spectrum	26 and 50 through 55
RAGS	Radiochemical analysis of gaseous samples	LLNL	Radioactive products	56
SRC (many)	Solid radiochemical collection diagnostic	LLNL/LANL	Radioactive products	57
WRF (many)	Wedged range filter	MIT/LLNL	Shell proton energy loss for deuterium-^{3}He implosions	58, 59, and 60

*Numbers in parentheses indicate the number of units.

TABLE VI

Diagnostics of Mix

Acronym	Diagnostic	Scientific Responsibility	Observable	Reference
Ross filter pair	Ross filter pair	LLNL	Mix	61
Super-snout II (multi-wavelength)	Multi-wavelength X-ray spectrometer	LLE/LLNL	Mix	62

Full Aperture Backscatter Station (FABS) and Near Backscatter Imager (NBI): The energy that is absorbed by the target is the input laser energy minus the light that leaves the target. For coherent light sources, most of the light leaving the target is back or forward scattered by stimulated Brillouin scattering (SBS) or stimulated Raman scattering (SRS). For X-ray drive targets, most of the laser energy that is not absorbed comes back into or close to the focusing lenses, which are arranged in sets of four (a quad) on NIF. The light backscattered into the lenses has a small transmission through the final turning mirror (which are 1ω mirrors) and is measured by the full aperture backscatter stations (FABSs) on two representative quads of the inner and outer beams (at 31 and 56 deg, respectively). Streak cameras connected to spectrometers in FABSs measure time and spectrally resolved stimulated Brillouin and Raman backscattering spectra SBS and SRS. These systems are called FABS31 and FABS56, respectively.[7]

In addition, some light is scattered in the area around the lenses and is measured by the three near backscatter imager (NBI) diagnostics on representative quads, an outer quad of beams at 50 deg, and two inner quads of beams, one at 31 deg and the other at 23.5 deg. The NBIs consist of spectralon scatter plates (see Fig. 3) surrounding the incident beam path and close to the target chamber wall, and a small scatter cross near the chamber wall between the beam apertures in one quad of beams at 23.5 deg. The intensity of light onto the scatter plates is observed from outside the target chamber through a view port with a line of sight to the scatter plates.

Broadband Time-Resolved X-Ray Spectrometer (Dante1 and Dante2): Dante1 and Dante2 are fixed soft X-ray power diagnostics mounted on the lower and upper hemispheres of the target chamber to see the inside of a hohlraum through its lower or upper LEH, respectively. Each Dante has 18 different spectrally and time-resolved channels. The spectral ranges are determined by the filter

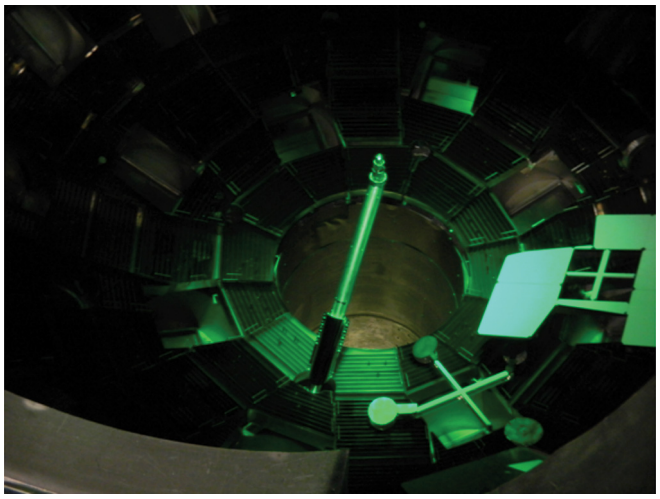

Fig. 3. Viewing the lower hemisphere of the NIF target chamber. The SPBT diagnostic is in the center on a fixed support coming in at 6:30 and is in a fixed position 2 m below the TCC. The scatter plates of NBI31 are on the right, and the scatter cross for NBI23.5 is at the bottom right.

packs and, for some channels, grazing incidence metallic mirrors. The delicate and expensive filters are mounted on a filter wheel (see Fig. 4), which is frequently replaced. The channels are centered at X-ray energies from 100 eV to ~10 keV. Dante1 has five mirrored channels, and Dante2 has eight mirrored channels.

Each channel is absolutely calibrated by measuring the diode sensitivity, mirror reflectivity, and transmission of its thin X-ray filters on a synchrotron source.[8,9] The photodiodes are connected through long cables to transient digitizers in electrically screened areas. The time resolution is ~150 ps after deconvolving the response function of the cables.

As shown in Fig. 4, the diodes are ~2 m outside of the NIF target chamber, 7 m from the target. Nevertheless, the X-ray flux on the soft channels can cause space charge saturation of the electron emission close to the photocathode. This effect is mitigated by achromatic attenuation of the X-rays by a 10% open area array of 50-μm holes in a disk placed at the location of the filter wheel so that the X-rays passing through the holes onto the photocathode are sufficiently diffracted and overlapping onto the photocathode to avoid local saturation.[10]

After spectral deconvolution Dante measures the X-ray power per steradian through a LEH. With knowledge of the size of the LEH, including its closure during a laser pulse measured by the SXIs, Dante determines the time-dependent radiation temperature in the hohlraum from the Stefan-Boltzmann law.

Filter Fluorescer (FFLEX): The filter fluorescer (FFLEX) diagnostic measures the absolute hard X-ray energy in ten spectral bands (15 to 400 keV) with time resolution initially implemented on two channels.[11] Figure 5 graphically illustrates the radial placement of the photomultipliers and scintillators that measure the light output from filtered fluorescers up to 100 keV for eight channels. The two hardest channels only have filters since no fluorescers are available >110 keV. Recently, all channels were upgraded to have time resolution.[12]

After deconvolution of the channel's impulse response function measured using a short-pulse laser system, the FFLEX time response is <400 ps. The absolute energy response of the photomultipliers and scintillators is measured at NSTec using a filtered fluorescer HEX source and absolutely calibrated detectors. The hard X-ray spectrum determines the "temperatures" and energy of hot electrons using a model of continuum X-ray emission from a spectrum of high-energy electrons. These energetic electrons

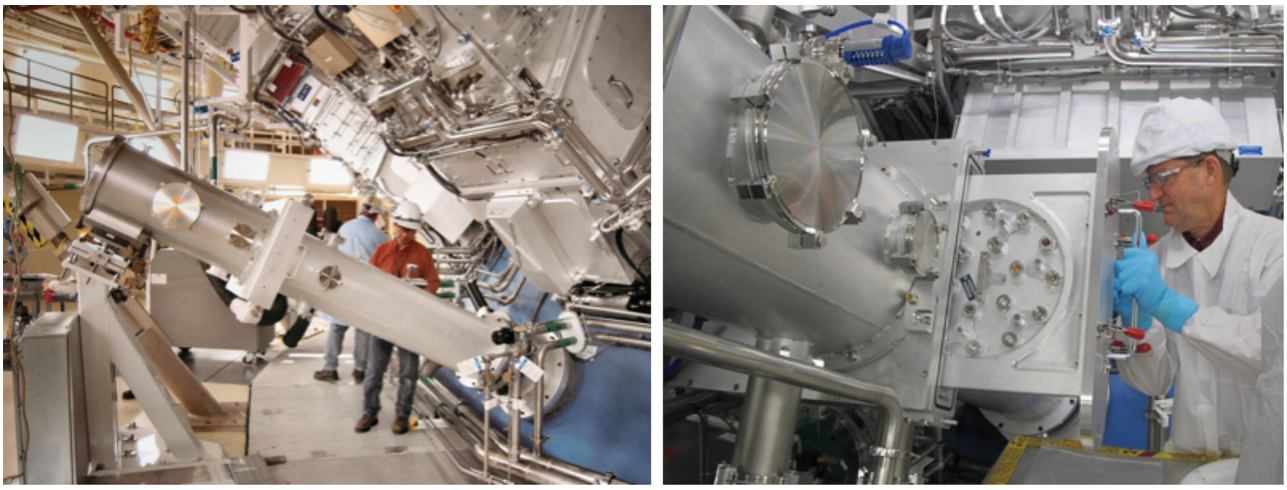

Fig. 4. The upper Dante diagnostic with a close-up of the Dante filter wheel being inserted, shown at right.

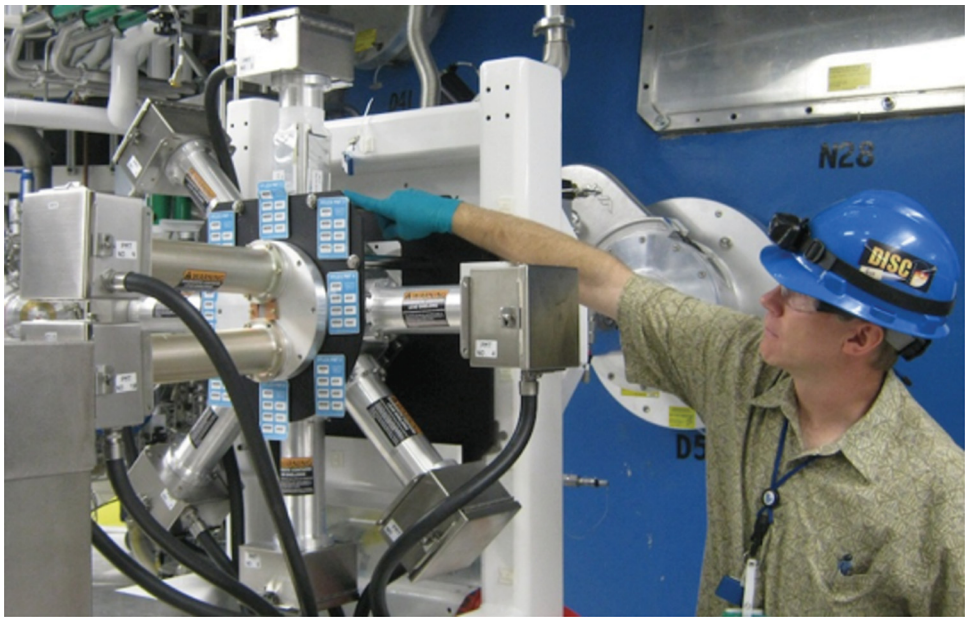

Fig. 5. The FFLEX X-ray diagnostic measures the hard X-ray spectrum. Shown are the eight radial direction channels, which were time integrated at the time of the NIC. Center-right are the two harder (higher-energy) channels, which are time resolved.

generated by laser-plasma instabilities (LPIs) can penetrate through the capsule ablator and preheat the deuterium-tritium (D-T) fuel, compromising fuel compression.[11]

Static X-Ray Imager (SXI) (SXI-U and SXI-L): Two static X-Ray imager (SXI) diagnostics [upper hemisphere (SXI-U) and lower hemisphere (SXI-L)] are mounted on retractable positioners and record multiple filtered pinhole images[13,14] of the target. On some channels, spectral selection is accomplished with filters and mirrors that provide low-resolution X-ray imaging at 900 eV. Other channels only use filters, providing 3- to 6-keV spectral imaging. The images are recorded on either image plates or CCDs, depending on the expected neutron yield. The locations of the SXIs were chosen to view the X-rays emitted from the inner walls of the hohlraums visible through the LEHs. This X-ray emission is used as a backlighter to measure the size of the LEH, although the image is weighted by the intensity of the hohlraum wall emission, most of which comes close to the end of an ignition-type pulse. The size of the LEH decreases during the pulse, and so, the measured LEH size is less than its original size.

The SXI was also one of the original diagnostics used to assist in the verification of laser pointing during NIF commissioning. These instruments can determine the positions of the laser spots focused on a planar target by measuring the resulting X-ray emission with respect to fiducial markings on the target.

Equatorial Hard X-Ray Imager (EHXI): The equatorial hard X-ray imager (EHXI) incorporates a static array of pinholes that forms many low-resolution, hard (>40-keV) X-ray images of hard X-rays transmitted through the hohlraum wall, the thermomechanical package (TMP) holding the multipart hohlraum together, and the thinned-out chamber flange. It is usually used to record low-resolution images of the positions of the beams striking the inside of the hohlraum. The pinhole array is outside of the chamber at ~6 m from the target with the image plate detector another 3 m farther away. The low-energy cutoff is set by the X-ray absorption in the hohlraum wall, the TMP, and a thinned-out target chamber flange. The data from the instrument, although graphic, is hard to use quantitatively. Arguably, it can resolve large errors in laser beam pointing and laser beam deposition.

Electromagnetic Power (EMP): The electromagnetic power (EMP) diagnostic measures the electromagnetic frequency spectrum in the target chamber. There is little documentation available for this diagnostic.

III.A.1. Comments on the NIF Drive Diagnostics

The laser absorption fraction is measured with adequate accuracy. With the NIC pulses the absorption was typically 80% to 85%. However, several aspects of the drive in the hohlraum should be improved. The Dante spectrometers only have a spectral resolution of about three to six. A crystal spectrometer with spectral

resolution about 100, viewing through the LEH, will improve the knowledge of the X-ray drive spectrum, particularly the fraction above 2 keV, and was performance qualified in 2015.

The LEH closes significantly during an implosion. There is a large loss of X-ray energy through the LEH, and so, knowledge of the time dependence of the closure is important. The SXIs use the natural backlighting from the hohlraum and take a time-integrated, emission-weighted measurement of the LEH size. Nanosecond time resolution on the SXI is being installed and will directly measure rather than model the closure rate of the LEH without relying on modeling. This capability was performance qualified in 2015.

There are no measurements of the plasma density and temperature in the NIF hohlraum. The spectra recorded by FABS from the SRS and SBS light depend on density and temperature but in a complex and hard-to-quantify manner. Optical Thomson scattering at about the fifth harmonic will enable time- and spatial-resolved measurements and will be available about 2018. Isoelectronic spectroscopy of tracer materials will give a measurement of the state of ionization and with modeling also give an electron temperature and became available in 2015.

III.B. Target Response/Implosion Diagnostics

The second class of diagnostics is the target response/implosion diagnostics. The capsule responds to the drive and implodes (or a planar target accelerates). The X-rays produced by the interaction of the laser beams with the inside wall of a hohlraum drive pressure waves that often steepen to shocks into the capsule within the hohlraum. As a result, the capsule is accelerated inward, causing the fuel inside to implode, and after an interval of time referred to as the "bang time" (BT), stagnate at the center of the shell. The uniformity and velocities of the shocks, the implosion velocity of the shell, the deviations from sphericity of the in-flight shell, the shape of the hot spot at stagnation, and the interval of time when stagnation occurs are measured with the set of diagnostics shown in Table III, which are categorized as response or implosion diagnostics.

Velocity Interferometer System for Any Reflector (VISAR) and Streaked Optical Pyrometer (SOP): The X-ray drive on a capsule or a planar target mounted on the side of a hohlraum produces a series of shocks, which needs to be delivered to the capsule at precise instants in time for ignition. An f/3 lens is held in the DIM at (90,315) to image the optical emission onto an optical streak camera. The break-out time of an optically emitting shock is measured with the SOP.

The same f/3 lens is also used for the Velocity Interferometer for Any Reflector (VISAR). The progress of the shocks through an optically transparent material (ablator or ice) is measured by the reflection of a probe laser beam off the shock wave into the f/3 lens (Fig. 6). The Doppler shift of the reflected light is measured by a Mach-Zender interferometer and a streak camera to obtain the time history of the velocity of the reflecting shock to high accuracies. The VISAR technique as used on a laser facility was developed extensively on OMEGA in the early 2000s (Refs. 15 and 16). VISAR has been very successfully used for shock timing up to the beginning of the fourth shock. A variant of the VISAR technique uses a tiny mirror mounted inside a capsule that allows viewing the inside wall of the capsule at two different positions simultaneously. This is referred to as the dual-axis VISAR technique.

DIM Insertable (X-Ray) Streak Camera (DISC): The trajectory (radius versus time for spherical targets, or position versus time for a planar experiment) of a target is measured with DIM insertable (X-ray) streak cameras (DISCs). These are X-ray streak cameras that have been designed to function in the harsh electromagnetic environment of the NIF target chamber.[17,18] In an X-ray streak camera, the X-rays are converted to photoelectrons in a transmission photocathode. Because the escape depth of photoelectrons is small compared to the X-ray absorption length of hard X-rays, the efficiency of streak cameras drops off significantly above 10 keV. Imaging is achieved by mounting a 15- to 25-μm space-resolving slit in 200-μm Ta, orthogonal to the time-resolving slit of the streak camera. The spatial magnification is set to about 10. Strong collimation is necessary to reduce hard X-ray backgrounds from hot electron–generated bremsstrahlung from the hohlraum walls. A bright uniform source of X-rays is placed behind the imploding target, and the position versus time of the shell is measured by the absorption of the backlighting X-rays by the target. An earlier version of the X-ray streak cameras established the initial beam synchronicity of arrival time at the target chamber center[17] (TCC). The X-ray streak cameras are used mainly to measure the position and width of the shell as a function of time using X-ray backlighting.[19] To monitor the fidelity of the streak rate and the timing, an ultraviolet 4ω fiducial, generated from a laser that is synchronous with the main laser, is transported by fibers to the X-ray streak camera and is displayed on the edge of the streak record.[20]

Time-Gated X-Ray Detector (GXD) and Hardened (Gated) X-Ray Imager (hGXI): When the imploded

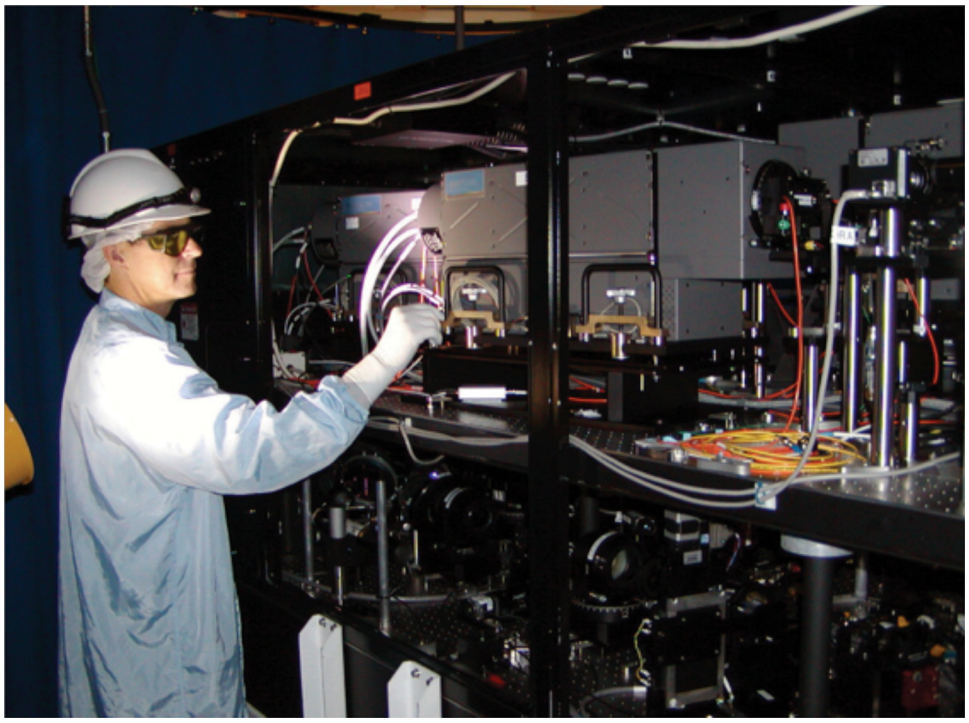

Fig. 6. Technician is shown aligning VISAR, an interferometer used to measure shock timing.

shell converges at its center, it heats, stagnates, and emits X-rays. The shape and time history of the X-ray emission depends in a complex way on the velocity and symmetry of the implosion and thus the intensity and symmetry of the X-ray drive. Measuring the evolution of the shape of the hot spot and drive symmetry by X-ray imaging is a technique that has been widely used in the ICF program for several decades.[21,22] The time-gated X-ray detector (GXD) instrument uses an array of pinholes projecting many images onto an electrically gated microchannel plate (MCP). Measurements are made at several times by coating several (typically four) conducting strips across the MCP. Typically, the active area of these detectors is located ~1 m from the TCC with the array of pinholes as close as 8 cm from the target. The array of hundreds of pinholes is laser drilled to a diameter of ~10 μm in a 100-μm-thick Ta disk, which is usually replaced every shot. Using an array of pinholes relaxes the alignment tolerance of the instrument to many hundred microns.

Time-gated X-ray detectors have evolved over many years to be sophisticated instruments with many control points.[25] GXDs use CCD detectors behind the gated MCPs and phosphors (Fig. 7). Data from the CCD are available immediately after a shot, but because of neutron-induced noise on the CCD, their use is limited to yield environments up to $\sim 10^{13}$ ×14.1 MeV neutrons per shot. To use gated X-ray imaging at a higher yield (up to about 10^{16} neutrons), hardened (gated) X-ray imagers (hGXIs) are used.[24] The main difference between the GXDs and the hGXIs is that the CCDs are replaced by optical film, which is less sensitive to neutrons. The electronics in the hGXIs are also much simpler than in the GXDs. Recent post-NIC work has examined subtle features of these gated instruments such as gain droop and cross-channel coupling effects that arise because different coated strips on the MCP are close to one another.[25]

Neutron Time-of-Flight Bang Time at 4 m (NTOF4BT): When the imploding target stagnates and heats, thermonuclear neutrons can be emitted for 100 to 200 ps, a short time compared to the implosion or run-in time of several nanoseconds. A neutron detector that is relatively close to the TCC can measure the time at which the burn or bang occurs. Measuring this time interval or

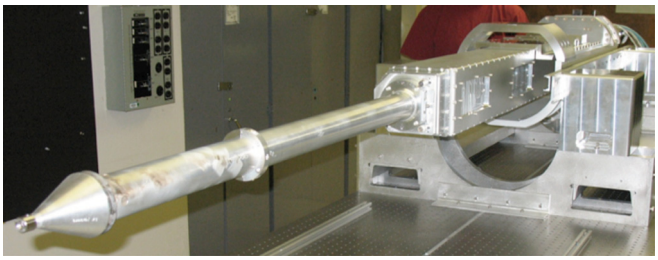

Fig. 7. Hardened gated X-ray imager with imaging snout attached. The hGXI is the rectangular box at the back. The pinhole assembly at the front (left) end of the snout is typically located 8 to 10 cm from the target.

Fig. 8. The PTOF detector is mounted on the side of the X-ray imaging snout. Here, a technician assembles a snout supporting three SRC detectors (top left and bottom) and a PTOF detector (top right) for an experiment. PTOF determines the timing of fusion production using a diamond detector that responds to neutrons and protons. The end of the snout has a pinhole array that is inserted on a DIM to ~10 cm from the NIF implosion. The assembly shown in this figure is attached to an air box that has a time-resolved detector such as a GXD or a DISC.

the BT helps to constrain the radiation drive. The neutron time-of-flight bang time at 4 m (NTOF4BT) detector[26] is housed in a short reentrant well in the target chamber 4 m from the target and measures the emission or BT of neutrons. This detector uses a diamond radiation-induced conductivity (RIC) detector and is closely coupled to a transient digitizer.

Proton (Particle) Time-of-Flight (PTOF) Detector: Some implosions on NIF have a gas fill of pure deuterium or deuterium and ^{3}He, producing 2.45-MeV neutrons from the deuterium-deuterium (D-D) fusion reaction and 14.7-MeV protons from the D-^{3}He fusion reaction. The time of peak fusion production for these reactions (BT) is measured with the proton (particle) time-of-flight (PTOF) detector[26,27] as shown in Fig. 8. As with the NTOF4BT, the detector uses the radiation- (particle-) induced conductivity in a synthetic diamond wafer detector.

As the PTOF is positioned on a DIM, the signal is recorded through ~150 ft of cable onto a transient digitizer. The BT time is determined by forward-fitting a Doppler-broadened particle source function convolved with the measured instrument response to the data. This technology has been extensively developed with direct-drive implosions on OMEGA and has demonstrated agreement with other NIF BT diagnostics on over 40 deuterium-tritium (D-T) neutron–producing implosions. Because of its fielding position 50 cm from the TCC, PTOF is the only NIF diagnostic capable of measuring BT using the lower-energy D-D neutrons and has measured BTs using neutron yields as low as 3×10^{10}. The sensitivity and proximity of the PTOF detector have allowed it to also provide both D-T and tritium-tritium (T-T) neutron BT measurements on hydrodynamic mix experiments and the D-D neutron BT measurement on a collision-less shock experiment.

For D-^{3}He–filled X-ray–driven implosions, the peak areal density can be high enough that the 14.7-MeV D-^{3}He protons produced during the main period of fusion reactivity (compression-bang) do not escape the implosion. But, before that time, the rebounding shock prior to peak compression can generate a period of fusion reactivity near the time of peak implosion velocity (shock-bang), when the areal density is low enough for protons to escape. If hard X-ray backgrounds are sufficiently low, the PTOF shielding is reduced so that these protons can be measured. The PTOF has measured the shock-BT using

D-^{3}He protons and the compression-BT using D-D neutrons on a recent near-vacuum hohlraum implosion with low X-ray background. This BT differential is an important forensic for the shock dynamics and hot spot adiabat of ICF implosions. In combination with wedged range filter (WRF)–measured areal density at shock-BT, the measured shock-BT will provide an important constraint on models of implosion dynamics.

To obtain a measurement of shock-BT and compression-BT from gas-filled hohlraum implosions with large hard X-ray backgrounds, an upgraded system [magnetic particle time of flight (MagPTOF)] will use a permanent magnet to deflect D-^{3}He protons around substantial X-ray shielding, improving the signal to background by three orders of magnitude.[28]

South Pole Bang Time (SPBT): The south pole bang time (SPBT) detector measures through the lower (south) hohlraum LEH the time of peak X-ray emission (peak compression) relative to the laser pulse of the implosion.[29] This interval, which is of the order of 20 ns from the start of the laser pulse for so called "low-foot" ignition implosions, is referred to as the "X-ray bang time." The instrument has a fixed X-ray RIC detector measuring the X-rays diffracted off a highly ordered pyroelectric graphite X-ray crystal at a distance of 2 m from the TCC. The Bragg angle of the crystal is set and filtered, so the SPBT is sensitive to a 1-keV band of X-rays centered at 10.8 keV and X-rays reflected in second order from the crystal. This instrument is also used for absolute measurements of the core emissivity as a measure of ablator impurity mix levels. Recently, a dedicated channel for second order (22 keV) has been added for inferring the free-free slope temperature of core X-rays. As well as the emission from the implosion, the instrument also records the X-rays from the hohlraum, which are distinguishable from the implosion by their longer characteristic timescale, and because in a well-designed implosion, the BT is longer than the laser pulse. Since the signal is relayed through several tens of meters of cable to an electrical recorder, the SPBT, like PTOF, can only measure the X-ray bang time to an accuracy of ~50 ps after cable deconvolution. Because of the loss of frequency response of the long cable, the SPBT cannot accurately measure the X-ray emission width of an implosion, the duration of which is on the order of 150 ps.

Streaked Polar Instrumentation for Diagnosing Energetic Radiation (SPIDER): The X-ray burn history from an implosion is measured by the Streaked Polar Instrumentation for Diagnosing Energetic Radiation (SPIDER). This is a fixed instrument mounted outside the chamber.[30] It measures the X-ray emission from an implosion at ~10 to 15 keV through the upper LEH at a viewing angle of 7 deg off vertical. At this angular deviation from the axis of the hohlraum, the capsule is still visible through the LEH of all hohlraums used so far. The detector is a DISC with a 4ω ultraviolet timing fiducial. An array of filters selects three or four different X-ray bands between ~8 and 15 keV across the length of the streak camera slit. This DISC is heavily shielded by polyethylene to allow the streak camera and instrument to operate up to D-T neutron yields of at least 10^{17}.

Gamma Reaction History (GRH): The achievement of higher neutron yields in NIF implosions provides robust statistics to obtain valuable high-quality nuclear diagnostic signatures such as the burn width, fuel areal density, and ion temperature. Since the nuclear data are more sensitive to the stagnated D-T fuel distribution, it complements well-established X-ray emission diagnostics.

The gamma reaction history (GRH) diagnostic measures the spectrum and time history of the emission of gamma rays produced from the D-T reaction and from gamma rays produced by neutrons interacting with matter.[31] In particular, neutrons inelastically scattering with carbon remaining from the ablator[32–34] are visible as a bright gamma line at 4.4. MeV. This is an outstanding example of a cold shell diagnostic. GRH detection of the 4.4-MeV gamma rays from the inelastic neutron scattering of ^{12}C (Ref. 32) supplies a direct measurement of the average remaining CH ablator areal density—a quantity difficult to deduce from X-ray emission because of opacity effects.

The GRH is set up with four threshold spectral channels. The channel responses are typically >2.9, >5, >8, and >10 MeV. In each GRH channel, gammas interact with an aluminum foil to produce Compton electrons, which recoil into a gas-filled cell. If the maximum velocity of the Compton electrons exceeds the speed of light in the cell adjusted by the pressure and temperature of the gas in the cell, they will generate a cone of broadband Cerenkov light. For each channel, Cerenkov light is relayed to a high-speed detector MCP photomultiplier, using a series of off-axis parabolic mirrors. This design incorporates a fixed time delay of 4.26 ns that allows the detector to recover from prompt radiation due to laser-plasma interactions from the target. The voltage signal from the photomultiplier is used to modulate a light signal via a Mach-Zehnder interferometer and then relayed with high fidelity to a digitizer. Figure 9 shows the GRH mounted on the outside of the NIF target chamber.

III.B.1. Comments on the Target Response Diagnostics

The implosion velocity is measured by radiography onto DISC as discussed above or by radiography onto a

Fig. 9. The GRH diagnostic is used to measure the time history gamma-ray emission. The four Cerenkov detectors are shown on the outside of the chamber.

gated camera. Implosion velocity is measured to adequate accuracy. However, it is important to measure drive asymmetry. Using self-emission, this is measured during the stagnation phase of an implosion. Measuring the drive asymmetry during the inward accelerating phase of an implosion requires measuring velocity differences around the limb of a few percent; this has not been possible so far. However, measuring asymmetry during the deceleration phase is now routinely done because the asymmetry is much larger at later time.

There is planned duplication in the BT diagnostics on the NIF. The SPBT diagnostic cannot measure the profile of X-ray emission because of its time response, whereas SPIDER can measure the time history of burn because it has a time resolution of ~30 ps. The neutron BT is not necessarily the same as the X-ray time, which is why NTOF4BT was built. GRH also measures the nuclear BT but with greater accuracy.

III.C. Fuel Assembly, Stagnation, and Heating Diagnostics

The third class of diagnostics is the fuel assembly, stagnation, and thermonuclear burn diagnostics. As the imploding fuel and remaining ablator approach the center of the capsule, they cause the pressure and temperature of the material at the center to rise forming a hot spot at temperatures of typically many kilo-electron-volts. This increase in pressure and temperature leads to deceleration and stagnation of the shell or ablator as well as the D-T fuel. Thermonuclear fusion reactions that produce high-energy neutrons, gammas, and alpha particles occur in the hot spot. NIF has a set of diagnostics to measure this phase of the implosion. The main attributes measured in this phase are categorized as being associated with

1. the hot spot (yield, hot spot size and shape, hot spot burn history, and hot spot electron and ion temperatures), Sec. III.C.1

2. diagnostics of the cold compressed fuel areal density, Sec. III.C.2
3. diagnostics of mix of the higher-density ablator into the hot spot, Sec. III.C.3. The suites of fuel assembly, stagnation, and heating diagnostics are shown in Tables IV, V, and VI.

III.C.1. Diagnostics of the Hot Spot

The neutron yield is a primary metric of the properties of the hot spot. For 14.1-MeV D-T neutrons, yield is measured by three independent absolute diagnostics, namely, two types of NADs and the MRS. These techniques are absolute in the sense that they depend on the known geometry, two different nuclear activation cross sections (copper and zirconium), and the neutron-proton or neutron-deuteron knock-on cross sections for the foil of the MRS. Because they have activation thresholds at 14 MeV, Cu and Zr are chosen as NAD materials, and so, downscattered neutrons will not cause activation. The levels of accuracy for all techniques are $<10\%$ and are only weakly dependent on yield for yields $>10^{13}$. The fact that the three independent techniques usually agree to $\sim 5\%$ adds confidence to estimates of accuracy.

For deuterium (D-D) and D-^{3}He gas fills, the lower-energy 2.4-MeV neutron yield is measured by neutron activation of an indium foil and/or absolute track counting in CR-39 samples exposed to the neutrons. Unfortunately, there is no threshold activation material for the D-D neutrons, so to minimize activation by scattering from the chamber, the indium NAD sample has to be held closely ($\sim$50 cm) to the target as shown in Fig. 8. As this detector is brought more closely to the neutron source, activation from the source dominates activation from scattering by mass in the chamber. The threshold nature of the activation detector materials Cu and Zr for 14.1-MeV neutrons does not have this background problem as scattering reduces the *n* energy enough that there is no activation.

A secondary diagnostic for D-T and D-D neutron yield immediately after a shot is provided by the NTOF detectors. These are secondary in that they are calibrated in situ against the three absolute detectors.

The diagnostics of yield, hot spot size and shape, hot spot burn history, and hot spot electron and ion temperatures are shown in Table IV and discussed below.

Neutron Activation Detector Using Copper (NAD-Cu): The neutron activation detector using copper (NAD-Cu) measures the unscattered neutron yield from D-T–filled capsules by activating copper foils.[35] Copper (and zirconium, discussed below) have high-energy thresholds for the (*n*,2*n*), so only the unscattered neutron yield is measured. Copper foils are installed in the neutron beam in both the Spec E and Spec A lines of sight. After the shot, foils are removed, and the activation level is determined using standard nuclear coincidence counting techniques. Because of the rapid decay rate of the activated copper (one half-life is 9.7 min), the foil must be quickly removed and counted in a detector system housed in the neutron alcove.

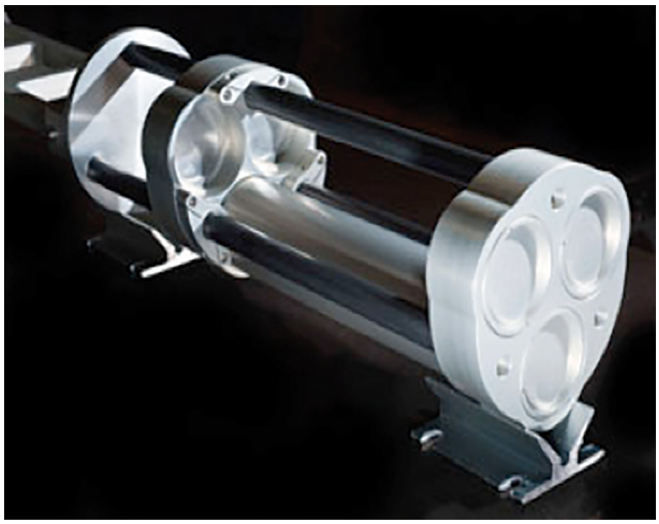

Fig. 10. The NAD in a well is designed to hold up to three zirconium samples at the front or back to measure the number of unscattered 14.1-MeV D-T neutrons.

Neutron Activation Detector in a Well Using Zirconium (NAD Well-Zr): The neutron activation detector in a well using zirconium (NAD Well-Zr) uses activation of a zirconium sample inserted into a short reentrant well on the target chamber as shown in Fig. 10 (Refs. 36 and 37). Zirconium, like copper, is an activation threshold detector for 14.1-MeV neutrons. Since the half-life of the zirconium activation product is 3.2 days, the counting facilities in the basement of building B151 at LLNL can be used to measure the level of activation.

Neutron Activation Detector DIM Mounted (NAD-Snout): For the 2.45-MeV neutrons produced in the D-D fusion reaction, indium is used as the activation detector. Because the indium 115(*n*,*n*') activation threshold is well below the neutron birth energy of 2.45 MeV, the sample needs to be close to the TCC to decrease the fractional contribution of scattering from the chamber. Consequently, the samples are mounted on DIM snout tubes, typically on the side of gated X-ray detectors mounted within the DIMs. The half-life of the indium activation product, 4.5 h, is comparable to the normal operational extraction time of a few hours, and so, the comprehensive LLNL radiochemistry counting facilities in building B151 can be also be used.[37]

Fig. 11. A technician installs a film pack in the ARIANE GXI for an experiment. ARIANE uses a CCD detector to electronically capture and record X-ray data for higher-yield experiments.

Active Readout In A Neutron Environment (ARIANE): The Active Readout In A Neutron Environment (ARIANE) gated X-ray imaging detector measures the X-ray hot spot size and shape up to a yield of $\sim 10^{17}$. ARIANE uses the gated MCP technology described for GXD and hGXI, but to operate in a higher neutron yield regime, the detector is moved farther away to a location just outside of the target chamber[38]; see Fig. 11. The pinhole array is held closely to the target by DIM (90,78), which is close in angle. A plan is in place to use a mirrored version of ARIANE for experiments for operation with yields in excess of 10^{17} neutrons.

Dilation X-Ray Imager (DIXI): The dilation X-ray imager (DIXI) drifts, and time dilates a photoelectron image of an implosion. The time dilation is achieved by ramping down the extraction field of the photoelectron image in a magnetic field.[39] Doing this causes early photoelectrons to spread out as they move down a drift tube from photoelectrons emitted later. The time-dilated image is then measured at the end of a drift tube in a solenoidal magnetic field with an MCP-based detector. The time dilation allows time resolution to >10 ps. This kind of time resolution is necessary because as the yield increases, the duration of X-ray emission should become <100 ps. At the end of NIC, this instrument was just being installed on the NIF having been tested on a smaller facility, but it did record NIF implosion data in 2014.

Neutron Imaging System (NIS): The neutron imaging system (NIS) creates static neutron images of the primary (14.1-MeV) unscattered D-T neutrons and the downscattered (6- to 12-MeV) neutrons from a burning D-T capsule. Images are formed through an array of neutron pinholes, but because of the 3.3-cm range of 14-MeV neutrons in the tungsten of the pinholes, the pinholes are precision-shaped grooves machined in 20 cm of gold plated on a tungsten substrate. Like many of NIF's diagnostics, neutron imaging was first demonstrated in the laboratory on Nova,[40] developed on OMEGA by LANL, LLE, and CEA staff,[41] and then installed on NIF (Refs. 42 and 43). The neutron pinhole array is held 32.5 cm from the TCC and aligned by the DIM 90-315 manipulator when not in use for VISAR and oriented by a precision articulating wrist. The neutron pinhole and its debris shield are shown in Fig. 12a.

The neutron image detector system is shown in Fig. 12b. It is located 28 m from the target in a building added onto the NIF for this purpose in 2011. The detector is a coherent fiber bundle of organic scintillator (BCF-99-55), but because of the nearly millimeter-range of the knock-on protons, a high magnification is required ($\sim$100X) to achieve $\sim$10-μm point-to-point source resolution. The primary unscattered neutron image is recorded by collecting light with a lens system from the front end of the scintillator fiber array onto a gated MCP optical detector,

(a) (b)

Fig. 12. (a) The front end of the NIS. The square object in the middle is the front end of the neutron pinhole array. The round object on the right is the debris shield in its open position to allow alignment. The other round object on the left is the converter foil for the MRS (Sec. III.C.2). (b) The detector end of the NIS located 28 m from the TCC. The neutrons travel from left-to-right through the detector system.

gated for the arrival time of the 14.1-MeV neutrons. The secondary scattered image is recorded by collecting light with a coherent fiber bundle from the back of the scintillator onto a second gated MCP optical detector gated for the arrival times of 6- to 12-MeV neutrons. The hot spot size and fuel asymmetry are determined from the image of the primary neutrons, and the cold fuel size and shape are inferred from the downscattered image.

Neutron Imaging Time of Flight (NITOF), Neutron Time of Flight at 20 m for Ignition (NTOF20IgHi), Neutron Time of Flight at 4 m (NTOF4) (3): With neutron yields larger than 10^{15} in current NIF implosions, we obtain high-quality nuclear diagnostic signatures such as the burn width, fuel areal density, and ion temperature, which are sensitive to the D-T fuel distribution. There are four separate NTOF detector types whose main function is to measure ion temperature of the hot spot from the thermal broadening of the neutrons. The spectrally resolving neutron imaging time of flight (NITOF), and NTOF20 SPECs described in Sec. III.C.2 also measure areal density. The neutron time of flight at 20 m for ignition (NTOF20IgHi) (Refs. 2, 6, and 44) is a chemical vapor deposition–based synthetic diamond detector located in the neutron alcove ~20 m from the TCC. The NITOF diagnostic is located upstream of the NIS system ~28 m from the TCC. These are far enough away from the target that the "thermal" broadening is large enough compared to the instrument response function that an accurate ion temperature measurement can be made. There are three neutron time-of-flight at 4 m (NTOF4) detectors mounted in short reentrant wells at the wall of the target chamber at a distance of ~4 m. One of the NTOF4 D-D detectors is configured with high sensitivity to measure D-D neutron yields as low as 10^9. Another two detectors, NTOF4 DT lo and NTOF4 DT hi, are configured to span the range of D-T neutron yields from 10^{11} to 10^{16}. These were relatively easy to install and were used early in NIC for approximate measurements of the ion temperature and over a large range of yields.

III.C.1.a. Comments on Hot Spot Diagnostics

The yield diagnostics give confidence in their errors because the different absolute techniques agree within several percentage points. As described above, the detector measures unscattered yield, excluding scattering from the cold fuel of the compressed target. For the layered implosion of NIC, a compressed D-T areal density of ~1 g/cm^2 was achieved that scatters ~20% of primary (14.1-MeV) neutrons. The Flange-NAD array of Sec. III.C.2 utilizes this effect.

The ability to measure the shape in the presence of yield is also adequate with caveats about the temporal and spatial resolution, and the X-ray opacity of the implosion. The principal ion temperature diagnostics are the NTOFs. The set at 4 m was installed early and has low resolution. The two at 20 m (Sec. III.C.2) do not adequately sample direction. A close-to-south-pole NTOF at ~20 m has now been fielded, and plans are in place for a close-to-north-pole NTOF at ~20 m.

III.C.2. Diagnostics of Areal Density of a Compressed Target

The hot spot model of ignition envisages a high-temperature, low-density region surrounded by a

low-temperature region at higher density in isobaric equilibrium with the hot spot. The areal density of the compressed shell that would mainly be D-T needs to be greater than ~1 g/cm^2 for ignition, which is much higher than ever before achieved in the laboratory. The diagnostics used to measure the critical parameter, the areal density of the compressed target, are shown in Table V.

Compton Radiography: Compton radiography (CR) is a measurement technique based on point-projection radiography at photon energies from 60 to 200 keV, where the Compton effect is the dominant contributor to the X-ray "opacity" (of course, photons are not absorbed but scattered). The advanced radiographic capability (ARC) will be a major enhancement to NIF giving it a short-pulse, high-power capability but was not available in 2013. ARC is a laser and is not described here. ARC will be used for time-resolved radiographic imaging of the dense cold fuel surrounding the hot spot by CR. Until ARC is available at NIF, CR with reduced resolution of ~30 μm is being performed using two focused 3ω quads of NIF (Ref. 45). The detector is a hardened, gated X-ray detector.

Magnetic Recoil Spectrometer (MRS): The magnetic recoil spectrometer (MRS) is a fixed-location neutron spectrometer that provides an accurate measurement of the neutron spectrum. Some of the hot spot D-T neutrons produced at 14.08 MeV are elastically scattered by compressed deuterium and tritium, which is assumed to be surrounding the hot spot. For example, a D-T areal density of 1 g/cm^2 elastically scatters ~20% of 14-MeV neutrons. The scattered neutrons emerge at a lower energy than 14 MeV and are a measure of the areal density. The fraction of neutrons downscattered into the 10- to 12-MeV region of the spectrum allows a measurement of compressed fuel areal density from the number and spectrum of downscattered neutrons. A MRS was first developed on OMEGA (Ref. 46). An updated version was installed on NIF in 2010 (Ref. 47) as shown in Fig. 1. D-T neutrons interact with a plastic foil (sometimes deuterated) held 30 cm from the target as shown in Fig. 12b, producing knock-on protons or deuterons. These charged particles are then dispersed by their momentum in a magnetic field and focused on an array of solid plastic film track detectors (CR-39) located at the focal point of the spectrometer. After a shot, the CR-39 is removed and etched, and the neutron spectrum and yield are determined by the location and number of tracks on the detectors.[48] The number of neutrons downscattered in energy by the compressed D-T is measured by the neutron spectrum. In addition, MRS records NIF's absolute unscattered yield[49] and ion temperature, although ion temperature is measured with lower resolution than the NTOF's, depending on the thickness of the plastic foil.

Flange Neutron Activation Diagnostic (Flange-NAD): The flange neutron activation diagnostic (Flange-NAD) is unique among NIF neutron diagnostics by making many simultaneous measurements of the same neutron source term from a particular shot.[37] Activity induced in up to 17 zirconium pucks at 17 different locations non-uniformly distributed around the target chamber through the Zr-90(n,2n)Zr-89 reaction is quantified by removing the pucks and detecting the 909-keV gamma ray from ^{89m}Y, the decay product of ^{89}Zr. Because the 3.2-day half-life of ^{89}Zr allows time for the physical removal of Zr samples, the gamma spectroscopy measurement is made using lead-shielded high-purity germanium detectors in a low-background counting facility. By careful design of the gamma spectroscopic measurement, the experimenter can in effect use the exact same instrument for all 17 simultaneous measurements, leaving only two major uncertainty components in the position-to-position activation ratio: the counting statistical variation and the shot-to-shot variability in the neutron source to activity transfer function. The relative uncertainty in the activation ratio between any two points can be reduced in practice to <2%, with the absolute D-T neutron yield measurement uncertainty near 7%. The anisotropy of the unscattered yield is measured from the variation of activation as a function of direction allowing for calibration factors. Any anisotropy in unscattered yield indicates a variation or asymmetry in the fuel areal density. Accurately measuring the anisotropy in the unscattered neutron yield from an implosion requires an accurate cross calibration using low areal density implosions because the compressed fuel areal density of ~1 g/cm^2 only downscatters ~20% of the 14-MeV neutrons, and variations in that 20% need to be measured accurately.

Neutron Time-of-Flight Spectrally Resolving Detector in the Alcove (NTOF20 SPEC A) and Neutron Time-of-Flight Spectrally Resolving Detector on the Equator (NTOF20 SPEC E): There are two neutron time-of-flight spectrometer (NTOF SPEC) detectors located at a distance of ~20 m from the TCC along widely spaced lines of sight, one in a well-shielded room called the alcove [neutron time-of-flight spectrally resolving detector in the alcove (NTOF20 SPEC A)] and one on the equator [neutron time-of-flight spectrally resolving detector on the equator (NTOF20 SPEC E)]. As the acronyms imply, they are designed primarily to measure the neutron spectrum and thus the ion temperature and downscattered neutron signals arriving after the primary neutron peaks for both 14- and 2.5-MeV neutrons. The technology for these spectrally resolving NTOFs was developed on

Fig. 13. Low mass neutron time-of-flight detector (center behind) is shown with instrument creators from LLNL.

OMEGA using liquid Xylene as a fast-decay scintillator.[50,51] Recently, that has been replaced by a Bibenzyl[52–54] crystal, which has an even faster decay but is as bright as the liquid and importantly is a solid. This feature then made possible an improved detector design (Fig. 13) that is very low mass and, as a result, creates very low scattering background. These lines of sight are well collimated by apertures preventing neutrons scattered off the target positioners, the DIM instruments, or the target chamber walls reaching the detectors. These detector improvements have enabled higher-precision data gathering and analysis of temperature, cold fuel scattering, and source velocity.[55] These instruments complement the MRS in measuring fuel areal density. Also, their location on the target chamber adds information about any anisotropy in areal density although the anisotropy in the downscattered signal is related in a complex way to the anisotropy in areal density.

Radiochemical Analysis of Gaseous Samples (RAGS) Diagnostic: The radiochemical analysis of gaseous samples (RAGS) diagnostic is used to collect and measure neutron activation products that are gaseous at room temperature.[56] For example, noble gases such as krypton and xenon can be used as activation detectors by preloading low levels of tracer materials into the ablator. The resulting krypton and/or xenon isotopes produced can be collected and chemically fractionated very efficiently by cryogenic trapping. Isotopic analysis of the collected samples, when corrected for contributions from air, can be used to obtain quantitative data on multiple capsule performance parameters such as mix of the shell material into the fuel, asymmetry of implosion, shell and fuel areal density at peak emission, and neutron yield. The apparatus is connected to the pumping system of NIF (see Fig. 14).

Solid Radiochemical Collection (SRC) Diagnostic: Neutron activation of the gold hohlraum is another example of a neutron-based probe of the stagnated shell conditions as embodied in the solid radiochemical collection (SRC) diagnostic.[57] The activated hohlraum debris is collected by SRC units placed ~50 cm from the TCC as shown in Fig. 7. The witness plates are removed after the shot and counted to determine the ratio of the $(n,\gamma)^{198}$Au capture to the $(n,2n)^{196}$Au product. The decay times of the two isotopes are 6 and 2 days, respectively, allowing remote counting. The neutron capture product is especially sensitive to low-energy neutron production, which is dominated by multiple scattering from the remaining compressed ablator hydrogen.[57] Thus, the ratio of the activated gold products is related to the areal density of the remaining ablator shell, supplying corroboration of the GRH ^{12}C measurement.[33]

Wedged Range Filters (WRFs): Wedged range filters (WRFs) are used to measure the energy spectrum of the protons from D-^{3}He gas-filled implosions.[58] The escaping thermonuclear protons primarily lose energy in the compressed ablator. When the areal density of the ablator is ~250 mg/cm^2 or higher, the protons are ranged out. As a result, the shock-produced protons produced earlier when the areal density is low are typically observed,

Fig. 14. The RAGS system collects and analyzes gases produced by NIF experiments.

while compression burn protons are ranged out. The energy spectrum of the escaping protons is measured by passing them through a wedge of material (see Fig. 15), after which the position and energy of the protons are recorded on a CR-39 track detector.[59] Between one and four WRF units are mounted at 50 cm from the TCC on each of the polar DIMs and equatorial DIMs (90-78). From the energy spectrum, the in-flight ablator ρR, ablator center-of-mass radius, and shock proton yield are inferred.[59] The technique yields valuable data prior to the full compression of the ablator. The combined polar and equatorial detectors also enable measurements of the in-flight low-mode ablator symmetry with this technique.[60]

Fig. 15. The WRF detector unit. The rectangle is a wedge of aluminum covering the plastic detector, which is CR-39. The cassette shown has a diameter of ~3 cm.

III.C.2.a. Comments on Diagnostics of Areal Density

At the beginning of NIC, it was hoped that CR would measure the shape of the areal density of the compressed fuel; however, the delay in the ARC laser has delayed the use of CR. As a result, during NIC the areal density was measured by neutron downscattering using two independent techniques of the NTOF SPEC and the MRS. The importance of areal density to ignition required two independent measurements that usually agree within the differences expected from the different lines of sight.

The issue with using neutron downscattering to measure areal density is that a measurement in a particular direction samples the areal density from a fraction of the shell defined by the direction of observation and the neutron scattering kinematics. For an ideal point source with an external shell, some deconvolution is possible; however, the accuracy of this assumption is not clear. During NIC, there were three measurements of areal density along the directions of NTOF SPEC A, NTOF SPEC E, and MRS chosen to cover reasonable anisotropy. In

Fig. 16. The Super-snout four-channel crystal spectrometer is attached to the recording box.

general, the values differed by 10% to 20%, and averages were taken. More NTOF SPECs are being planned.

Both NTOF SPEC and MRS make measurements of ion temperature and areal density, which are time integrated weighted by yield over the implosion. Plans are being made for a time-dependent MRS to give ion temperature and areal density measurements with ~30-ps resolution during an implosion.

III.C.3. Diagnostics of Mix

Ross Filter Pairs: An array of "Ross filtered" pinholes produces many time-integrated X-ray images detected by image plates. Several different filter packs in the energy range from 8 to >20 keV (Ref. 61) using the Ross pair matching technique are used to produce many images in this energy region. These give measures of the temperature- and density-sensitive bremsstrahlung emission from the imploding core. These data provide estimates of hot spot mass, mix mass, and pressure, as well as broadband, time-integrated absolute X-ray self-emission images of the imploded core.

Multi-Wavelength X-Ray Spectrometer (Super-Snout): Two four-channel curved crystal spectrometers are used to record with medium spectral resolution the K shell X-rays from elements such as germanium or copper. These materials are added as dopants into the plastic ablators, and if the ablator mixes into the hot spot, the K lines, principally He-like, of the dopants emit X-rays. The intensity of the X-ray lines is an indicator of the density and temperature of the mixed emission region.[62] The spectrometer is a snout that is attached to the front of a gated detector, and the data are recorded onto an image plate as shown in Fig. 16. Like many other NIF diagnostics, this instrument was developed and tested at OMEGA before installation on the NIF.

IV. LOCATIONS OF DIAGNOSTICS ON THE NIF TARGET CHAMBER

The locations of the target positioners (TarPos, and CryoTarPos), DIMs, and some of the diagnostic systems on the NIF target chamber are shown in Fig. 17. Also shown in Fig. 17 are the final optics damage inspection system (FODI) and the opposed port alignment system (OPAS).

V. TARGET DIAGNOSTICS, CONTROL SYSTEMS, AND INFRASTRUCTURE

Controls for target diagnostics are managed as part of the Integrated Computer Control System (ICCS) high-level architecture.[63] ICCS incorporates over a thousand front-end processors, servers, and workstations to control,

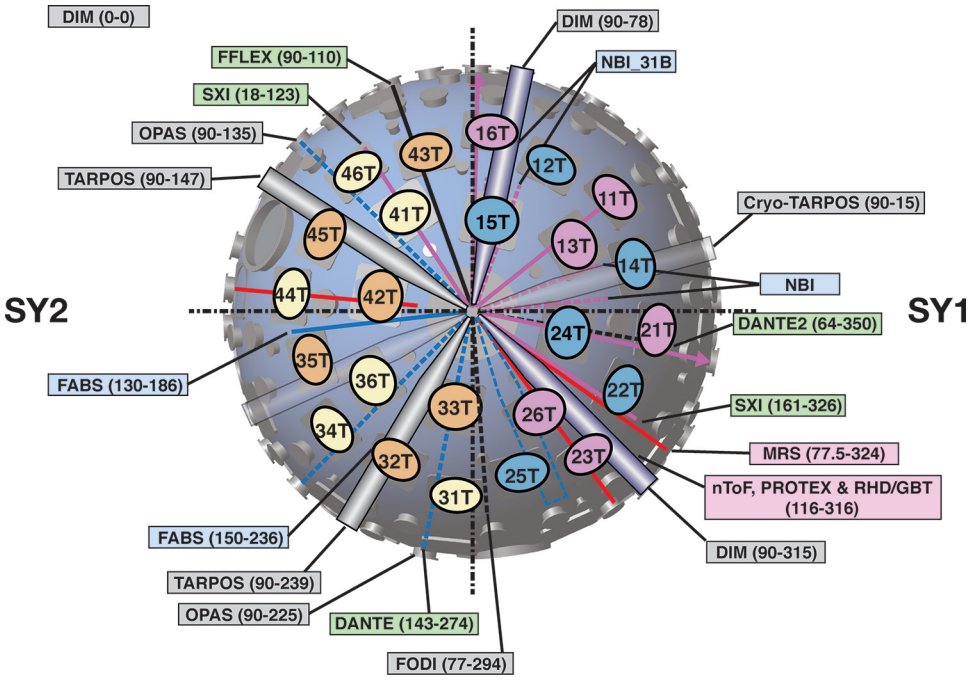

Fig. 17. Top view of the NIF target chamber, showing the location of 24 of the quads of laser beams (labeled such as 42T, etc.) and some of the diagnostics. The quads come from the switchyards, SY1 and SY2 (shown on the right and left, respectively) and are reflected into the chamber by mirrors not shown. NIF diagnostics are either constructed and deployed to a fixed location in the target chamber/bay or are fielded on a DIM.

diagnose, and fire the laser, as well as to integrate the suite of target diagnostics. ICCS is described in more detail in the paper "Control and Information Systems for the National Ignition Facility," also in this special issue of *Fusion Science and Technology*. Target diagnostics have unique control system requirements; they must be able to operate outside of the supervisory environment and be operated or calibrated in facilities other than NIF.

During NIC, the target diagnostics embedded control architecture was modified to use a single low-cost PC104 processor per device (e.g., a digitizer). The full diagnostic control is then composed within the supervisory software by aggregating the network-attached controllers. This approach simplifies the embedded software, improves reliability, and provides easy reuse of devices in other diagnostics.

V.A. Diagnostic Control System

The diagnostic control system (DCS) framework for NIF hardware and software was developed to

1. reduce hardware and software costs
2. increase efficiency by reusing software
3. improve verification and test case coverage
4. speed up development turnaround for new diagnostics.

Each complex diagnostic typically uses an ensemble of electronic instruments attached to sensors, digitizers, cameras, and other devices. A diagnostic's supporting instruments (i.e., power supplies, cameras, and/or digitizers) are each maintained by a dedicated computer controller with generic DCS software customized to that instrument. Figure 18 illustrates this architecture for the Dante soft X-ray spectrometer diagnostic. The Dante diagnostic uses one DCS controller with software and interface hardware specific to the power supply and 20 more controllers with software and interface specific to the oscilloscope. The various DCS computers are located in standard 19-in. electronic racks in one of four diagnostic mezzanines adjacent to the NIF target area shielding wall, along with the power supplies and digitizers. Computers are connected to the ICCS network through network switches in the diagnostic mezzanine. These controllers are diskless and boot from a file server over the network. Experimental data collected from cameras and digitizers by each controller are sent to the file server for processing and archiving.

Figure 19 illustrates the DCS framework, which instantiates objects that perform the following common functions. In the DCS architecture, each instrument is interfaced to a low-cost Windows processor and JAVA application. The JAVA framework provides data

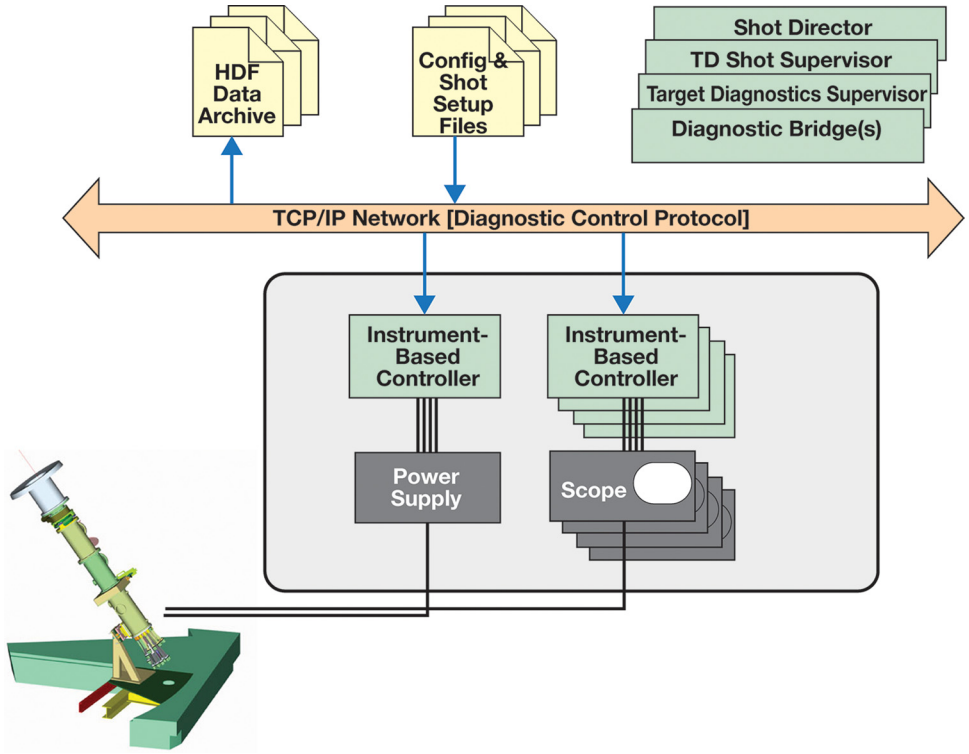

Fig. 18. The DCS architecture as applied to the Dante X-ray diagnostic.

management, control services, and operator GUI generation. DCS instruments are reusable by replication with reconfiguration for specific diagnostics in extensible markup language. Advantages include minimal application code, easy testing, and high reliability. Collaborators save costs by assembling diagnostics with existing DCS instruments.

V.B. Target Diagnostic Supervisor

The ICCS target diagnostic subsystem is a target diagnostic front-end processor containing diagnostic bridges and supervisory and shot control software. Diagnostic bridges translate DCP protocol messages from each DCS instrument into ICCS CORBA-distributed objects.

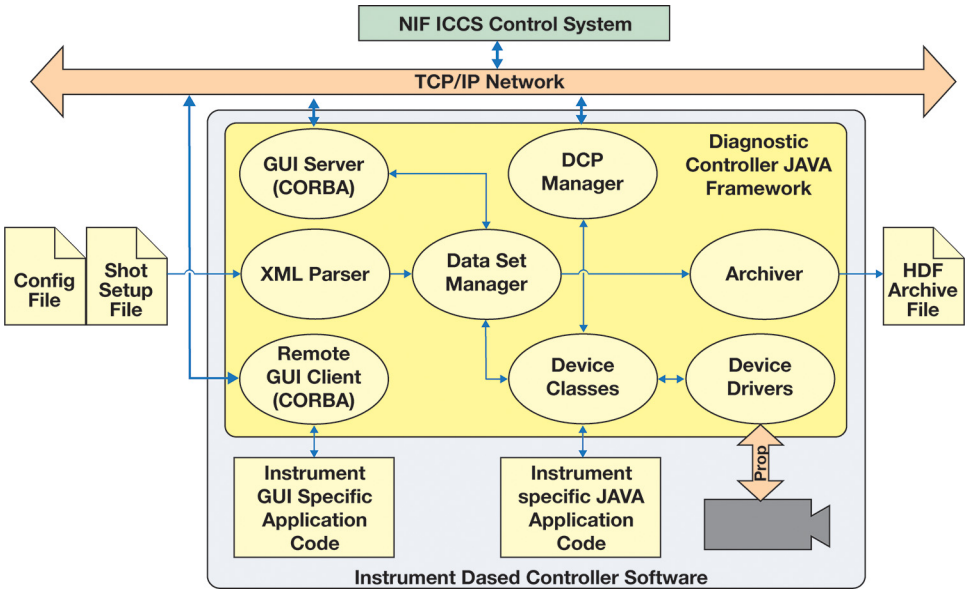

Fig. 19. The DCS framework.

The target diagnostic supervisor uses these bridges to provide status and control of each DCS instrument and groups the set of instruments for the diagnostics they support. The target diagnostic supervisor also provides the primary operator interface at the target diagnostic console in the control room. The shot supervisor executes macrosteps that are defined in a shot model for participating diagnostics on any given shot. Instrument configuration for a specific diagnostic and shot combination is established in configuration files by the responsible diagnostic engineer. After review of the postshot data from a given diagnostic by the responsible diagnostic engineer, it is made available to the user via the Archive Viewer.[64]

V.C. Diagnostic Timing Infrastructure

The NIF is a complex system of lasers and diagnostics. In order to successfully drive a target, the beams must be synchronized as they arrive at the target, and in order to successfully acquire diagnostic data of the physics experiment, the target diagnostics must be triggered at the appropriate time to record the event of interest. Further, to interpret the data, it is necessary to have a timing monitor system from which the actual timing may be inferred. From the target diagnostics, this is referred to as the cross-timing system.

The timing for the NIF beams is established in the master oscillator room (MOR), where 48 individual triggers from the integrated timing system initiate the 48 different pulse generators. A separate trigger initiates a fiducial pulse that is then distributed passively throughout the facility as a timing reference. This fiducial pulse is a 1ω optical pulse that is split and amplified, and distributed either directly by fiber or via optical-to-electrical (O-E) converters to the laser power diagnostics and target diagnostics and cross-timing system.

The implementation of the cross-timing system varies with instrument type. For the laser power sensors, the fiducial is delivered to an O-E converter and recorded on the same transient digitizer record that captures the laser power. There are 12 digitizers that record pulse shapes and the fiducial pulse for all of NIF. For optical streak cameras such as those implemented in the VISAR diagnostic, the fiducial is delivered directly to the photocathode adjacent to the data window, and it is recorded on the same image as the data itself. For gated X-ray imagers, the transient pulses that provide the gate windows for each strip line are multiplexed and delivered to a transient digitizer as a monitor pulse. The fiducial pulse is recorded on a separate channel of the same digitizer, providing a reference that can be linked back to the laser timing.

Timing is first established using impulses. The laser is configured to drive a gold-coated plastic sphere with 88-ps impulses. Target diagnostics are configured to record the X-ray and optical signal associated with the high-intensity lasers striking the target. The timing of the individual instruments is interpreted and compared to the fiducial to provide a reference offset that can be interpreted as the time-zero timing. For an optical streak camera, the time of the fiducial is determined relative to time zero, where the data are known by association with the laser pulse timing. For a gated X-ray imager, the time the instrument triggered is inferred based on the location of the data recorded on the strip line, and then, the timing of the monitor pulse relative to the fiducial is used to define a monitor reference time that would correspond to the instrument triggering at time zero.

By using a series of target shots to initially establish the reference times for each instrument, the actual timing of the target diagnostic data may be inferred to <50 ps relative to the laser pulse. This allows for correlation of nuclear versus X-ray versus optical data, and also correlation of data recorded from multiple different lines of sight simultaneously.

VI. COMPARISON OF NIF AND NOVA DIAGNOSTICS

It is interesting to compare the diagnostic set on Nova in the late 1990s and NIF as detailed above. Nova was activated about 1984, and so, the comparison is between a

TABLE VII

Comparison of Optical Spectrometers and Imagers for NIF and the Ten-Beam Chamber of Nova

Optical Diagnostics	Nova	NIF
Streaked optical pyrometer	SOP	SOP
Streaked interferometer	VISAR	VISAR
Streaked optical spectrometers	SOS, BSS	
Multiple streaked spectroscopy	MATRES	
Spatially discriminating optical streaked spectrograph	SDOSS	
Calorimeter array	EBM	
Full beam backscatter	SOS5	FABS
Near backscatter	NBI	NBI
Thomson scattering	$2w$, $4w$	

TABLE VIII

Comparison of X-Ray Imagers for NIF and the Ten-Beam Chamber of Nova

X-Ray Imagers	Nova	NIF
Wolter X-ray microscope	22x	
Gated X-ray pinhole camera	GXI, WAX, GACS, GSIX	GXD, hGXI
Axial pinhole cameras	APH	Polar GXD
Low-resolution imagers	Kirkpatrick Baez microscopes-8X	SXI-U&L
Neutron-hardened gated imager		ARIANE, DIXI
Hard X-ray imager		EHXI
Gated soft X-ray framing camera	SXRFC	Snout
Streaked soft X-ray imager	NSDSS	Snout
Ring aperture microscope	RAM	
Streaked slit/array imager	SSC/SMP	DISC

TABLE IX

Comparison of X-Ray Spectrometers for NIF and the Ten-Beam Chamber of Nova

X-Ray Spectrometers	Nova	NIF
Streaked crystal spectrometers	NSCS, Keanetech 2	NXS
High-resolution streaked spectrometer	HICKS	
Static crystal spectrometers	Henway, POS	
High-resolution crystal spectrometers	HOPS	
Gated crystal spectrometer	TOPS	Super-snout
Gated imaging extreme ultraviolet spectrometer	IXUVS	
Laue spectrometer	HETS	TARDIS
Low-resolution X-ray diode array	Dante	Dante
Low-resolution high-energy fluorescers	FFLEX	FFLEX

mature facility and a relatively new facility. Nova had a ten-beam and a two-beam chamber. The comparison here is for the ten-beam chamber of Nova.[1] The two-beam chamber was mostly used for X-ray laser research and so had some very specialized soft X-ray spectrometers.

Table VII shows that NIF is missing some of the optical diagnostics that Nova had, particularly Thomson scattering to measure plasma density and temperature. Concepts are being developed to put 5ω optical Thomson scattering on NIF in a few years' time to measure the density and temperature inside hohlraums. The energy balance module systems (EBMs) on Nova were set up to measure scattered light at many locations. There are some discussions to make an equivalent diagnostic for NIF for direct drive, but it is not recognized as being of high value at the moment especially as the so-called DrD laser backscatter diagnostics measure backscatter into the lenses.

Nova had both KirkPatrick Baez (KB) and Wolter X-ray reflective optics, as shown in Table VIII. However, these were designed during the planning phase of Nova before it was realized that on Nova pinhole arrays functioned well. There are plans for a KB and, in the long term, a Wolter on NIF mainly because of the need to go to harder X-ray imaging utilizing the new technology of ultrasmooth X-ray reflecting layers for hard X-rays. The ring aperture imaging on Nova allowed for high spatial resolution, but in practice it was rarely used. NIF does have one item of new technology with drift tube technology, which was installed on NIF but not demonstrated on NIF until about 2014.

NIF has been relatively slow in fielding X-ray spectrometers but is comparable to Nova in its lower-resolution ($R < 1000$) capability, as shown in Table IX. There are plans to build a higher-resolution spectrometer for NIF in the medium term. NIF had no soft X-ray capability at the end of NIC, but X-ray transmission capability was introduced recently.

The neutron diagnostic suites on Nova and NIF as shown in Table X are broadly comparable considering the lower areal density on Nova. Nova had two high-resolution single-hit spectrometers: LANSA and the LANL Ti neutron spectrometer. These were used to measure the Doppler broadening of the primary neutrons and to measure the secondary D-T spectrum from D-D implosions. Because the yield is higher on NIF, the NITOF SPECs and the MRS accurately make these measurements

TABLE X

Comparison of Neutron and Gamma Diagnostics for NIF and the Ten-Beam Chamber of Nova

Neutron Diagnostics	Nova	NIF
Yield	Cu and In NAD	Cu, Zr, and In NAD
Yield anisotropy		Zr NAD-Flange
Bang time	NETMCP, GaAs	NTOF4BT
Medium-resolution neutron spectrometer	NTOF	NTOF4, NTOF SPEC
Ultrahigh-resolution spectrometer	fNTOF	NITOF
Burn history (*n*,X-ray)	NTD and GaAs	GRH, SPBT, SPIDER
High-resolution neutron spectrometer	LANSA	
High-resolution high-sensitivity spectroscopy	LANL Ti	
Neutron spectrometer		MRS
Proton spectrometer		WRF, PTOF
Neutron imager	NPAM	NIS
Solid collection	SIM	SRC
Rapid collection	Rabbit	
Gaseous collection		RAGS

and more. A single-hit detector for high-resolution, low-energy neutron spectroscopy on NIF has been discussed, but there are no plans at the moment.

The neutron burn profile diagnostic on Nova was the neutron temporal detector (NTD), which uses a scintillator close to the target and an optical streak camera to differentiate the fast-rising and relatively slow-falling optical scintillation. This instrument then went to OMEGA. In contrast, the higher yield of NIF allowed the use of the low-emission rate of the 17-MeV fusion gammas using GRH. A quantitative comparison of NTD and GRH from OMEGA is still under study.

VII. SUMMARY AND CONCLUSION

The history of the 36 different types of NIF diagnostics is described in Sec. I, highlighting the role of the whole U.S. ICF community. A history of scientific cooperation on diagnostics has been documented in the proceedings in the *Review of Scientific Instruments* of the long-lived HTPD conferences. In making the case for the NIF, the JCDT, a national management team, formulated the plan for NIF diagnostics, which it documented in the NIF CDR. These diagnostics proposed two decades ago were all installed on the NIF with small changes. The NIF diagnostic capability is broadly equivalent to Nova's in 1999. NIF diagnostics have a greater degree of automation than Nova's, and many have been upgraded to operate in the harsher EMP/X-ray and higher neutron environment produced by NIF hohlraums and implosions, respectively. The rigorous design and commissioning process has contributed to an extremely reliable suite of diagnostics on the NIF, delivering high-quality data >99% of the time. A comprehensive summary of all of the NIF diagnostics is given in the bulk of this paper in Sec. III. As NIF moves forward, scientific innovation is beginning to show up in NIF diagnostics, such as in DIXI, and a range of concepts for new diagnostics is being explored.

APPENDIX

ACRONYMS

ARC = advanced radiographic capability

AWE = Atomic Weapons Establishment

ARIANE = Active Readout In A Neutron Environment

CCD = charge-coupled device

CDR = conceptual design report

CEA = Commissariat à l'Energie Atomique

CR = Compton radiography

Dante = broadband, time-resolved X-ray spectrometer

DCS = diagnostic control system

D-D = deuterium-deuterium

DIM = diagnostic insertion manipulator

DISC = DIM insertable (X-ray) streak camera

DIXI = dilation X-ray imager

D-T = deuterium-tritium

EBM = energy balance module system

EHXI = equatorial hard X-ray imager

EMP = electromagnetic power

EP = execution plan

FABS = full aperture backscatter station

FFLEX = filter fluorescer

Flange-NAD = flange neutron activation diagnostic

FODI = final optics damage inspection system

GA = General Atomics

GRH = gamma reaction history

GXD = time-gated X-ray detector

GXI = time-resolved X-ray imager

hGXI = hardened (gated) X-ray imager

HEX = high-energy X-ray

HTPD = High Temperature Plasma Diagnostic (conference)

ICCS = Integrated Computer Control System

ICF = inertial confinement fusion

JCDT = Joint Central Diagnostic Team

KB = KirkPatrick Baez

LANL = Los Alamos National Laboratory

LANSA = large area neutron scintillator array

LEH = laser entrance hole

LLE = Laboratory for Laser Energetics

LLNL = Lawrence Livermore National Laboratory

MCP = microchannel plate

MIT = Massachusetts Institute of Technology

MRS = magnetic recoil spectrometer

NAD = neutron activation detector

NAD Well-Zr = neutron activation detector in a well using zirconium

NAD-Cu = neutron activation detector using copper

NAD-snout = neutron activation detector DIM mounted

NBI = near backscatter imager

NI = neutron imager

NIC = National Ignition Campaign

NIF = National Ignition Facility

NIS = neutron imaging system

NITOF = neutron imaging time of flight

NSTec = national securities technology

NTC = Nova Technical Contract

NTD = neutron temporal detector

NTOF = neutron time of flight

NTOF SPEC = neutron time-of-flight spectrometer

NTOF20 SPEC A = neutron time-of-flight spectrally resolving detector in the alcove

NTOF20 SPEC E = neutron time-of-flight spectrally resolving detector on the equator

NTOF20IgHi = neutron time of flight at 20 m for ignition

NTOF4 = neutron time of flight at 4 m

NTOF4BT = neutron time-of-flight bang time at 4 m

OPAS = opposed port alignment system

PQ = Performance Qualification

PTOF = proton (particle) time-of-flight (detector)

RAGS = radiochemical analysis of gaseous samples (diagnostic)

RIC = radiation-induced conductivity

SBS = stimulated Brillouin scattering

SDOSS = spatially discriminating optical streaked spectrograph

SID = system for insertable diagnostics

SIM = six-inch manipulator

SNL = Sandia National Laboratories

SOP = streaked optical pyrometer

SPBT = south pole bang time

SPIDER = Streaked Polar Instrumentation for Diagnosing Energetic Radiation

SRC = solid radiochemical collection (diagnostic)

SRS = stimulated Raman scattering

SSC = streaked slit camera

Super-snout = multi-wavelength X-ray spectrometer

SXI = static X-ray imager

SXRI = soft X-ray imager

SXSS = soft X-ray streak spectrometer

TCC = target chamber center

TIM = ten-inch manipulator

TMP = thermomechanical package

VISAR = Velocity Interferometer System for Any Reflector

WRF = wedged range filters

YN = neutron yield

Acknowledgment

This work was performed under the auspices of the U.S. Department of Energy by Lawrence Livermore National Laboratory under contract DE-AC52-07NA27344.

References

1. J. D. KILKENNY, "Recent Diagnostic Developments at Nova (Invited)," *Rev. Sci. Instrum.,* **63**, 4688 (1992); http://dx.doi.org/10.1063/1.1143610.
2. "National Ignition Facility Conceptual Design Report," UCRL-PROP-117093 Vol. 2, NIF-LLNL-94-113 L-16973-1, Lawrence Livermore National Laboratory (May 1994).
3. J. D. KILKENNY et al., "Diagnostic Systems for the National Ignition Facility (NIF) (Invited)," *Rev. Sci. Instrum.,* **66**, 288 (1995); http://dx.doi.org/10.1063/1.1146387.
4. E. M. CAMPBELL et al., "Recent Results from the Nova Program at LLNL," *Laser Part. Beams,* **9**, 209 (1991); http://dx.doi.org/10.1017/S0263034600003293.
5. R. J. LEEPER et al., "Target Diagnostic System for the National Ignition Facility," *Rev. Sci. Instrum.,* **68**, 868 (1997); http://dx.doi.org/10.1063/1.1147917.
6. T. J. MURPHY et al., "Neutron Time-of-Flight and Emission Time Diagnostics for the National Ignition Facility," *Rev. Sci. Instrum.,* **72**, 850 (2001); http://dx.doi.org/10.1063/1.1321001.
7. J. D. MOODY et al., "Backscatter Measurements for NIF Ignition Targets," *Rev. Sci. Instrum.,* **81**, 10D921 (2010); http://dx.doi.org/10.1063/1.3491035.
8. E. L. DEWALD et al., "Dante Soft X-Ray Power Diagnostic for National Ignition Facility," *Rev. Sci. Instrum.,* **75**, 3759 (2004); http://dx.doi.org/10.1063/1.1788872.
9. K. M. CAMPBELL et al., "Omega Dante Soft X-Ray Power Diagnostic Component Calibration at the National Synchrotron Light Source," *Rev. Sci. Instrum.,* **75**, 3768 (2004); http://dx.doi.org/10.1063/1.1789603.
10. R. E. TURNER et al., "Achromatically Filtered Diamond Photoconductive Detectors for High Power Soft X-Ray Flux Measurements," *Rev. Sci. Instrum.,* **70**, 656 (1998); http://dx.doi.org/10.1063/1.1149385.
11. E. L. DEWALD et al., "Hot Electron Measurements in Ignition Relevant Hohlraums on the National Ignition Facility," *Rev. Sci. Instrum.,* **81**, 10D938 (2010); http://dx.doi.org/10.1063/1.3478683.
12. M. HOHENBERGER et al., "Time-Resolved Measurements of the Hot-Electron Population in Ignition-Scale Experiments on the National Ignition Facility (Invited)," *Rev. Sci. Instrum.,* **85**, 11D501 (2014); http://dx.doi.org/10.1063/1.4890537.
13. M. B. SCHNEIDER et al., "Images of the Laser Entrance Hole from the Static X-Ray Imager at NIF," *Rev. Sci. Instrum.,* **81**, 10E538 (2010); http://dx.doi.org/10.1063/1.3491316.
14. M. B. SCHNEIDER et al., "Soft X-Ray Images of the Laser Entrance Hole of Ignition Hohlraums," *Rev. Sci. Instrum.,* **83**, 10E525 (2012); http://dx.doi.org/10.1063/1.4732850.

15. P. M. CELLIERS et al., "Line-Imaging Velocimeter for Shock Diagnostics at the OMEGA Laser Facility," *Rev. Sci. Instrum.,* **75**, 4916 (2004); http://dx.doi.org/10.1063/1.1807008.
16. R. M. MALONE et al., "Overview of the Line-Imaging VISAR Diagnostic at the National Ignition Facility," *Proc. SPIE,* **6342** (2007); http://dx.doi.org/10.1117/12.692236.
17. J. R. KIMBROUGH et al., "Standard Design for National Ignition Facility X-Ray Streak and Framing Cameras," *Rev. Sci. Instrum.,* **81**, 10E530 (2010); http://dx.doi.org/10.1063/1.3496990.
18. Kentech Instruments Ltd. Web Site: http://www.kentech.co.uk/index.html?/&2 (current as of Oct. 3, 2015).
19. E. L. DEWALD et al., "Capsule Ablator Inflight Performance Measurements Via Streaked Radiography of ICF Implosions on the NIF," *Proc. 8th Int. Conf. Inertial Fusion Sciences and Applications (IFSA 2013)*, Nara, Japan, September 8–13, 2013 (2014).
20. Y. P. OPACHICH et al., "X-Ray Streak Camera Cathode Development and Timing Accuracy of the 4ω Ultraviolet Fiducial System at the National Ignition Facility," *Rev. Sci. Instrum.,* **83**, 10E123 (2012); http://dx.doi.org/10.1063/1.4732855.
21. J. D. KILKENNY et al., "High-Speed Gated X-Ray Imagers (Invited)," *Rev. Sci. Instrum.,* **59**, 1793 (1988); http://dx.doi.org/10.1063/1.1140115.
22. G. A. KYRALA et al., "Measuring Symmetry of Implosions in Cryogenic Hohlraums at the NIF Using Gated X-Ray Detectors," *Rev. Sci. Instrum.,* **81**, 10E316 (2010); http://dx.doi.org/10.1063/1.3481028.
23. J. A. OERTEL et al., "Gated X-Ray Detector for the National Ignition Facility," *Rev. Sci. Instrum.,* **77**, 10E308 (2006); http://dx.doi.org/10.1063/1.2227439.
24. P. M. BELL et al., "Radiation Hardening of Gated X-Ray Imagers for the National Ignition Facility," *Rev. Sci. Instrum.,* **81**, 10E540 (2010), http://dx.doi.org/10.1063/1.3491208; see also N. IZUMI et al., "Experimental Study of Neutron Induced Background Noise on Gated X-Ray Framing Cameras," *Rev. Sci. Instrum*., **81**, 10E515 (2010), http://dx.doi.org/10.1063/1.3478636.
25. L. R. BENEDETTI et al., "Crosstalk in X-Ray Framing Cameras: Effect on Voltage, Gain, and Timing (Invited)," *Rev. Sci. Instrum.,* **83**, 10E135 (2012); http://dx.doi.org/10.1063/1.4740524.
26. V. YU. GLEBOV et al., "The National Ignition Facility Neutron Time-of-Flight System and Its Initial Performance," *Rev. Sci. Instrum.,* **81**, 10D325 (2010); http://dx.doi.org/10.1063/1.3492351.
27. H. G. RINDERKNECHT et al., "A Novel Particle Time of Flight Diagnostic for Measurements of Shock- and Compression-Bang Times in D3He and DT Implosions at the NIF," *Rev. Sci. Instrum.,* **83**, 10D902 (2012); http://dx.doi.org/10.1063/1.4731000.
28. H. G. RINDERKNECHT et al., "A Magnetic Particle Time-of-Flight (MagPTOF) Diagnostic for Measurements of Shock- and Compression-Bang Time at the NIF (Invited)," *Rev. Sci. Instrum.,* **85**, 11D901 (2014); http://dx.doi.org/10.1063/1.4886775.
29. D. H. EDGELL et al., "South Pole Bang-Time Diagnostic on the National Ignition Facility (Invited)," *Rev. Sci. Instrum.,* **83**, 10E119 (2012); http://dx.doi.org/10.1063/1.4731756.
30. S. F. KHAN et al., "Measuring X-Ray Burn History with the Streaked Polar Instrumentation for Diagnosing Energetic Radiation (SPIDER) at the National Ignition Facility," *Proc. SPIE,* **8505** (2012); http://dx.doi.org/10.1117/12.930032.
31. H. W. HERRMANN et al., "Diagnosing Inertial Confinement Fusion Gamma Ray Physics," *Rev. Sci. Instrum.,* **81**, 10D333 (2010); http://dx.doi.org/10.1063/1.3495770.
32. N. M. HOFFMAN et al., "Measurement of Areal Density in the Ablators of Inertial-Confinement-Fusion Capsules Via Detection of Ablator (n, n0c) Gamma-Ray Emission," *Phys. Plasmas,* **20**, 042705 (2013); http://dx.doi.org/10.1063/1.4799799.
33. D. B. SAYRE et al., "Multi-Shot Analysis of the Gamma Reaction History Diagnostic," *Rev. Sci. Instrum.,* **83**, 10D905 (2012); http://dx.doi.org/10.1063/1.4729492.
34. C. CERJAN et al., "Gamma Reaction History Ablator Areal Density Constraints upon Correlated Diagnostic Modeling of National Ignition Facility Implosion Experiment," *Phys. Plasmas,* **22**, 032710 (2015); http://dx.doi.org/10.1063/1.4916124.
35. G. W. COOPER et al., "Copper Activation Deuterium-Tritium Neutron Yield Measurements at the National Ignition Facility," *Rev. Sci. Instrum.,* **83**, 10D918 (2012); http://dx.doi.org/10.1063/1.4746999.
36. C. B. YEAMANS, D. L. BLEUEL, and L. A. BERNSTEIN, "Enhanced NIF Neutron Activation Diagnostics," *Rev. Sci. Instrum.,* **83**, 10D315 (2012); http://dx.doi.org/10.1063/1.4739230.
37. D. L. BLEUEL et al., "Neutron Activation Diagnostics at the National Ignition Facility," *Rev. Sci. Instrum.,* **83**, 10D313 (2012); http://dx.doi.org/10.1063/1.4733741.
38. V. SMALYUK et al., "X-Ray Imaging in an Environment with High-Neutron Background on National Ignition Facility," *Proc. SPIE,* **8144**, 81440N (2011); http://dx.doi.org/10.1117/12.894200.
39. S. R. NAGEL et al., "Dilation X-Ray Imager a New/Faster Gated X-Ray Imager for the NIF," *Rev. Sci. Instrum.,* **83**, 10E116 (2012); http://dx.doi.org/10.1063/1.4732849.
40. D. B. RESS et al., "Neutron Imaging of Laser Fusion Targets," *Science,* **241**, 956 (1988); http://dx.doi.org/10.1126/science.241.4868.956.
41. L. DISDIER et al., "Neutron Imaging of ICF Target Plas-

mas (Invited)," *Rev. Sci. Instrum.,* **74**, 1832 (2003); http://dx.doi.org/10.1063/1.1534931.

42. F. E. MERRILL et al., "The Neutron Imaging Diagnostic at NIF (Invited)," *Rev. Sci. Instrum.,* **83**, 10D317 (2012); http://dx.doi.org/10.1063/1.4739242.
43. E. N. LOOMIS et al., "Progress Toward the Development and Testing of Source Reconstruction Methods for NIF Neutron Imaging," *Rev. Sci. Instrum.,* **81**, 10D311 (2010); http://dx.doi.org/10.1063/1.3492384.
44. R. A. LERCHE et al., "National Ignition Facility Neutron Time-of-Flight Measurements," *Rev. Sci. Instrum.,* **81**, 10D319 (2010); http://dx.doi.org/10.1063/1.3478680.
45. R. TOMMASINI et al., "Development of Compton Radiography of Inertial Confinement Fusion Implosions," *Phys. Plasmas,* **18**, 056309 (2011); http://dx.doi.org/10.1063/1.3567499.
46. J. A. FRENJE et al., "Probing High Areal-Density Cryogenic Deuterium-Tritium Implosions Using Down-Scattered Neutron Spectra Measured by the Magnetic Recoil Spectrometer," *Phys. Plasmas,* **17**, 056311 (2010); http://dx.doi.org/10.1063/1.3304475.
47. M. GATU JOHNSON et al., "Neutron Spectrometry—An Essential Tool for Diagnosing Implosions at the National Ignition Facility," *Rev. Sci. Instrum.,* **83**, 10D308 (2012); http://dx.doi.org/10.1063/1.4728095.
48. D. T. CASEY et al., "The Coincidence Counting Technique for Orders of Magnitude Background Reduction in Data Obtained with the Magnetic Recoil Spectrometer at OMEGA and the NIF," *Rev. Sci. Instrum.,* **82**, 073502 (2011); http://dx.doi.org/10.1063/1.3605483.
49. D. T. CASEY et al., "Measuring the Absolute Deuterium-Tritium Neutron Yield Using the Magnetic Recoil Spectrometer at OMEGA and the NIF," *Rev. Sci. Instrum.,* **83**, 10D912 (2012); http://dx.doi.org/10.1063/1.4738657.
50. V. YU. GLEBOV et al., "Prototypes of National Ignition Facility Neutron Time-of-Flight Detectors Tested on OMEGA," *Rev. Sci. Instrum.,* **75**, 3559 (2004); http://dx.doi.org/10.1063/1.1788875.
51. V. YU. GLEBOV et al., "The National Ignition Facility Neutron Time-of-Flight System and Its Initial Performance (Invited)," *Rev. Sci. Instrum.,* **81**, 10D325 (2010); http://dx.doi.org/10.1063/1.3492351.
52. R. HATARIK et al., "Characterizing Time Decay of Bibenzyl Scintillator Using Time Correlated Single Photon Counting," *Rev. Sci. Instrum.,* **83**, 10D911 (2012); http://dx.doi.org/10.1063/1.4732178.
53. V. YU. GLEBOV et al., "Testing a New NIF Neutron Time-of-Flight Detector with a Bibenzyl Scintillator on OMEGA," *Rev. Sci. Instrum.,* **83**, 10D309 (2012); http://dx.doi.org/10.1063/1.4731001.
54. J. A. BROWN et al., "Relative Light Yield and Temporal Response of a Stilbene-Doped Bibenzyl Organic Scintillator for Neutron Detection," *J. Appl. Phys.,* **115**, 193504 (2014); http://dx.doi.org/10.1063/1.4878238.
55. J. D. KILKENNY et al., "Antipodal Neutron Time of Flight (nToF) Detectors More Than Double Their Diagnostic Value," *BAPS,* **59**, *15*, BO412 (2014).
56. D. A. SHAUGHNESSY et al., "The Radiochemical Analysis of Gaseous Samples (RAGS) Apparatus for Nuclear Diagnostics at the National Ignition Facility (Invited)," *Rev. Sci. Instrum.,* **83**, 10D917 (2012); http://dx.doi.org/10.1063/1.4742145.
57. D. A. SHAUGHNESSEY et al., "Radiochemical Determination of Inertial Confinement Fusion Capsule Compression at the National Ignition Facility," *Rev. Sci. Instrum.,* **85**, 063508 (2014), http://dx.doi.org/10.1063/1.4883186; see also C. HAGMANN et al., "Note: Radiochemical Measurement of Fuel and Ablator Areal Densities in Cryogenic Implosions at the National Ignition Facility," *Rev. Sci. Instrum*., **86**, 076105 (2015), http://dx.doi.org/10.1063/1.4926743.
58. A. B. ZYLSTRA et al., "Charged-Particle Spectroscopy for Diagnosing Shock ρR and Strength in NIF Implosions," *Rev. Sci. Instrum.,* **83**, 10D901 (2012); http://dx.doi.org/10.1063/1.4729672.
59. A. B. ZYLSTRA et al., "The Effect of Shock Dynamics on Compressibility of Ignition-Scale NIF Implosions," LLNL-JRNL-657078, Lawrence Livermore National Laboratory (July 14, 2014).
60. A. B. ZYLSTRA et al., "In-Flight Observations of Low-Mode ρR Asymmetries in NIF Implosions," *Phys. Plasmas,* **22**, 056301 (2015); http://dx.doi.org/10.1063/1.4918355.
61. T. MA et al., "Imaging of High-Energy X-Ray Emission from Cryogenic Thermonuclear Fuel Implosions on the NIF," *Rev. Sci. Instrum.,* **83**, 10E115 (2012); http://dx.doi.org/10.1063/1.4733313.
62. S. P. REGAN et al., "Applied Plasma Spectroscopy: Laser-Fusion Experiments," *High Energy Density Phys.,* **5**, 234 (2009); http://dx.doi.org/10.1016/j.hedp.2009.05.004.
63. R. T. SHELTON et al., "Target Diagnostic Control System Implementation for the National Ignition Facility," *Rev. Sci. Instrum.,* **81**, 10E101 (2010); http://dx.doi.org/10.1063/1.3464576.
64. M. S. HUTTON et al., "Experiment Archive, Analysis, and Visualization at the National Ignition Facility," *Fusion Eng. Des.,* **87**, 2087 (2012); http://dx.doi.org/10.1016/j.fusengdes.2012.07.009.